THESIS FOR THE DEGREE OF LICENTIATE OF ENGINEERING

Ultra-thin Niobium Nitride Films for Hot Electron Bolometer and THz Applications

Sascha Krause

Group for Advanced Receiver Development
Department of Earth and Space Science
Chalmers University of Technology
Gothenburg, Sweden 2016

Ultra-thin Niobium Nitride Films for Hot Electron Bolometer and THz Applications
Sascha Krause

Thesis for the degree of Licentiate of Engineering

Group for Advanced Receiver Development
Department of Earth and Space Science
Chalmers University of Technology
SE-412 96 Gothenburg
Sweden
Telephone + 46 (0)31-772 1000

Cover:
Upper left corner: The Atacama Path Finder Experiment representing the exploration of space in the submillimeter and THz frequency range, upper right corner: HRTEM image of ultra-thin NbN film that is grown onto a GaN buffer-layer in an epitaxial manner, lower left corner: SEM image of the employed HEB used for measuring the phonon escape time, lower right corner: Resistance versus temperature behavior of the investigated ultra-thin NbN films which were grown onto different buffer-layers and substrates.

[Printed by Chalmers Repro Service]
Gothenburg, 2016

Ultra-thin Niobium Nitride Films for Hot Electron Bolometer and THz Applications

Sascha Krause

Group for Advanced Receiver Development
Department of Earth and Space Science
Chalmers University of Technology
Gothenburg, Sweden 2016

Abstract

The part of the electromagnetic spectrum between microwaves and infrared, also known as the terahertz band, is of particular interest for radio astronomy. The radiation intensity of the cold universe peaks at this frequency band, thus defining the demand on sensitive low-noise instruments in this particular frequency range. Phonon-cooled hot electron bolometers based on niobium nitride (NbN) thin films have been demonstrated for the first time in 1990 and evolved since then to the technology of choice for frequencies above 1.2 THz. At those wavelengths their noise temperature is typically between 5 to 10 times the quantum noise hence outperforming any other heterodyne receiver technology. However, the main concern of HEBs is there limited intermediate frequency (IF) of, in practice a few GHz, which is not sufficient for certain astronomical tasks requiring, e.g. 4-12 GHz of bandwidth. The cooling rate of "hot" electrons translates directly into the IF bandwidth of such devices and is intrinsically determined by the quality and thickness of the used NbN film and the substrate, which serves as a heat sink in these phonon-cooled devices [1].

This thesis deals with the development of NbN films particularly for the use in hot electron bolometers, and is addressing the optimization of superconducting properties of the NbN ultra-thin films. A particular emphasis was put on the influence of the underlying substrate. The suitability of hexagonal $Al_xGa_{1-x}N$ as a buffer-layer for the NbN film growth was demonstrated for the first time and enabled the tuning of the superconducting properties by changing the Al content x. Single crystal NbN with 5 nm thickness has been grown onto GaN with T_c of 13.2 K, very narrow superconducting transition width and residual resistivity ratio (R_{20K}/R_{300K}) close to unity. The critical current density J_c was determined to be 3.8MA/cm^2, compared to 1.2MA/cm^2 of a high quality NbN film deposited onto a silicon substrate.

The GaN buffer-layer is also believed to result in improved acoustic matching compared to commonly used substrates such as silicon or MgO, thus possibly enhancing the IF bandwidth. A first mixer experiment, where the HEB was operated in the bolometric mode at 180 GHz and at elevated bath temperatures, showed clearly that the measured IF roll-off, which is associated with the phonon escape time in this mode of operation was increased almost by 80% while the GaN buffer-layer was used as compared to a bare silicon substrate.

Keywords: Hot electron bolometers, epitaxial growth, NbN, GaN, IF bandwidth

List of Appended Papers

This thesis is based on the following papers:

A S. Krause, D. Meledin, V. Desmaris, A. Pavolotsky, V. Belitsky, M. Rudzinski and E. Pippel, "Epitaxial growth of ultra-thin NbN films on $Al_xGa_{1-x}N$ buffer-layers," Supercond. Sci. Technol., vol. 27, no. 6, Apr 2014.

B S. Krause, V. Afanas'ev, V. Desmaris, D. Meledin, A. Pavolotsky, V. Belitsky, A. Lubenschenko, A. Batrakov, M. Rudzinski, E. Pippel, "Ambient temperature growth of mono- and polycrystalline NbN nanofilms and their surface and composition analysis," Submitted to Transactions on Applied Superconductivity.

Other publications

The following publications are not appended at the end of the thesis due to overlapping content.

S. Krause, D. Meledin, V. Desmaris, A. Pavolotsky, V. Belitsky, E. Pippel, "Deposition of high-quality ultra-thin NbN films at ambient temperatures", International Symposium on Terahertz Technology, 2014.

V. Afanas'ev, S. Krause, A. V. Lubenchenko, A. A. Batrakov, V. Desmaris, A. B. Pavolotsky, V. Belitsky, "Study of NbN ultra-thin films for THz hot-electron bolometers", International Symposium on Terahertz Technology, 2014.

S. Krause, D. Meledin, V. Desmaris, A. Pavolotsky, V. Belitsky, E. Pippel, "Ultra-thin film NbN depositions for HEB heterodyne mixer on Si-substrates", International Symposium on Terahertz Technology, 2013.

Acknowledgments

First of all, I would like to thank Prof. Victor Belitsky, who put his trust in me by giving me the opportunity of the PhD study as well as the continuous support since I started. In addition to that, I could always count on my supervisors Assoc. Prof. Vincent Desmaris and Dr. Denis Meledin who made time for me whenever I needed it and I am glad to not only call them my working colleagues. I gained much understanding from discussions with Alexey Pavolotsky and Hawal Rashid as well as the whole GARD team that has been very supportive throughout my time here and I am convinced that they keep doing that in the future.
I am grateful over the fruitful collaboration with Dr. Mariusz Rudzinski at the Institute of Electronic Materials Technology Epitaxy Department, Warsaw, Poland who provided constantly numerous AlGaN epi-layers for the prospective deposition of high quality NbN ultra-thin films as being subject of this thesis.
The HRTEM images taken by Dr. Eckhard Pippel at the Max-Planck-Institute fuer Mikrostrukturphysik in Halle, Germany gave me insight in structures on an atomic level and have been of great help in this work.
Besides the scientific support, I would like to thank my fantastic friends, Lotti and my dear family, without them I most likely haven't come so far in life.

Sascha Krause
Gothenburg, January 2016

Contents

List of Abbreviations and Symbols

ALMA	Atacama Large Millimeter Array
SIS	Superconductor - Insulator - Superconductor
HEB	Hot electron bolometer
THz	Terahertz
GHz	Gigahertz
MHz	Megahertz
RF	Radio frequency
IF	Intermediate frequency
LSB	Lower side band
USB	Upper side band
SNR	Signal to noise ratio
DC	Direct current
LO	Local oscillator
LNA	Low noise amplifier
IVC	Current voltage curve
BCS	Bardeen - Cooper - Schrieffer
GLAG	Ginzburg - Landau - Abrikosov - Gor'kov
HRTEM	High resolution transmission electron microscopy
HAADF	High angle annular dark field
STEM	Scanning transmission electron microscopy
XRD	X-Ray diffraction
REELS	Reflection electron energy loss spectroscopy
MOCVD	Metal organic chemical vapor deposition
NbN	Niobium nitride
NbTi	Niobium titanium
NbO_2	Niobium dioxide
Nb_2O_5	Niobium-II-pentoxide
AlGaN	Aluminum gallium nitride
GaAs	Gallium arsenide
MgO	Magnesium oxide
SiC	Silicon carbide
Si	Silicon
SiO_2	Silicon dioxide
SOI	Silicon on insulator
fcc	Face centered cubic
LHe	Liquid helium
ADS	Agilent Advanced Design System
DUT	Device under test

List of Notations

Notation	Description	Unit
C	Capacitance (electrical), capacity (thermal)	F, J K^{-1}
c_e, c_{ph}	Specific capacity of electrons, phonons	J kg^{-1} K^{-1}
k_{ph}	Specific thermal conductivity of phonons	W m^{-1} K^{-1}
P	Power	W
E	Energy, electric field strength	J, V m^{-1}
ΔE	Energy shift	J, eV
S	Sensitivity	V/W
I	Current, intensity	A
J_c	Critical current density	A m^{-2}
V	Voltage	V
R	Resistance	Ohm
ρ	resistivity	kg m^3 s^{-3} A^{-2}
RRR	Residual resistance ratio R_{300K}/R_{20K}	-
T_c	Critical temperature	K
ΔT	Transition width	K
H_{c2}	Second critical magnetic Field	A m^{-1}
B	Magnetic flux density	Wb m^{-2}
d	Thickness	M
l, l_e	Length, electron mean free path	m
Λ	Phonon mean free path	m
w	Width	m
f	Frequency	Hz
ω	Angular frequency	rad s^{-1}
v_t, v_l	Acoustic velocity transverse, longitudinal	m s^{-1}
v_F	Fermi velocity	m s^{-1}
ϵ_F	Fermi energy	kg m^2 s^{-2}
ρ_F	Fermi momentum	kg m s^{-1}
N(0)	Density of states	m^{-3}
Θ	Debye temperature	K
γ	Sommerfeld constant	J m^{-3}
$\tau_{e\text{-}ph}$, τ_{esc}	Relaxation time electron-phonon, escape	s
β_l, β_t	Kinetic constant longitudinal, transverse	m s^{-1}
λ	Wavelength, London penetration depth	m
η	Efficiency	-
α	Transmission coefficient	-
a	Lattice constant	Å

1
Background

1.1 Radio astronomy receivers in the submillimeter and THz range

Astronomy is considered a science, which originated with the appearance of mankind itself. The observation of processes taking place outside Earth's atmosphere has been done for thousands of years with the bare eye and still has not lost any of its interest. With the invention of the telescope in 1608 [2], the development of more sensitive instruments has just been initiated.
The frequency range between approximately 300 GHz and 10 THz, usually referred to the sub-millimeter and THz range is, compared to the visible part of the electromagnetic spectrum or the microwave region, strongly absorbed in the atmosphere, in particular by water vapor in the troposphere as illustrated in Figure 1. In order to deal with the weak signals, ground based observation sites specialized in the observation in this frequency range, have been established at higher altitudes such as the Atacama Path Finder Experiment (APEX) in 5104 m [3], the Submillimeter Telescope Observatory (SMTO) in 3180 m [4], the SAO Receiver Lab Telescope (RLT) in 5500 m [5] or the advanced Atacama Large Millimeter/Submillimeter Array (ALMA) in 5000 m which is being established in a global collaboration [6] and profit from the higher atmospheric transmissivity.
Despite the small fraction of this radiation that passes our atmosphere, approximately 50 % of all present photons in the cosmos belong to the submillimeter and THz frequency range [7]. It harbors a vast amount of spectral lines, which are associated with rotational transitions of molecules and atomic transitions of ionized gases. For astronomical tasks, the transitions of CO are of particular interest [8]. Moreover, the energy emitted by cold matter in the form of

black body radiation peaks in this frequency band and provides insight in processes like the formation of stars.
The corresponding wavelength of THz radiation, similarly to microwaves, is still long enough to barely interact with interstellar dust grains and therefore, allow for the survey of areas in space which are concealed for visible light.

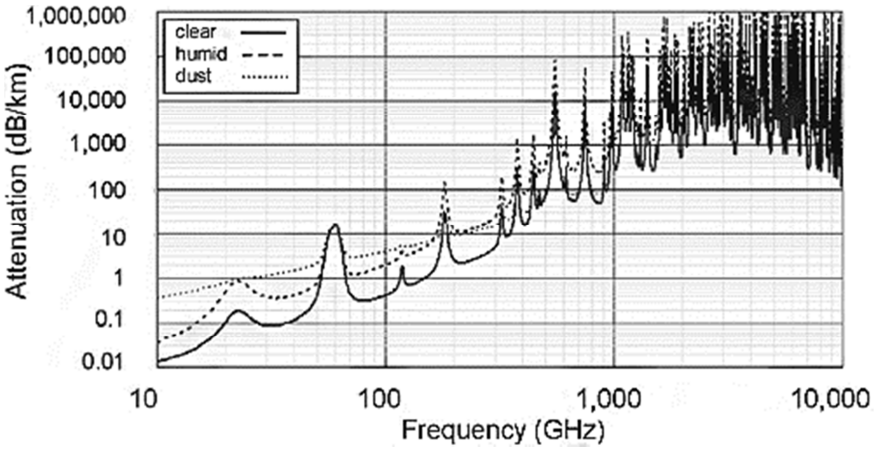

Figure 1: Atmospheric absorption versus frequency under different atmospheric conditions. The distinct peaks are associated with rotational transitions of molecules and ionized atoms [9].

The investigation of emission lines in the spectrum of interstellar objects requires heterodyne receivers featuring high spectral resolution as well as ultimate sensitivity due to the weak signal levels. In the last decades, frequency mixers based on superconducting material such as the SIS [10] and the HEB [11] have been developed and enable ground based spectroscopy, capable of resolving distinct spectral lines of different molecules and atomic transitions.
In common heterodyne receivers operating at microwave frequencies, there will be a low noise amplifier (LNA) at the frontend of the receiver chain to amplifier the RF signal before it is down-converted in the mixer. The LNA adds noise to the signal but all noise contributions from the following receiver components are reduced by the gain of the amplifier. With increasing operating frequency, however, the gain of the amplifier decreases and its noise contribution rises, which in turn deteriorates the overall noise temperature of the receiver tremendously. It is therefore beneficial and a necessity at THz frequencies to place a mixer directly at the frontend of the receiver.
Schottky diodes can be employed in the whole sub-millimeter and THz band but perform poorly from a noise perspective compared with the superconducting technologies and require higher LO power level to be pumped. Nonetheless they can also be operated without the need of cooling.

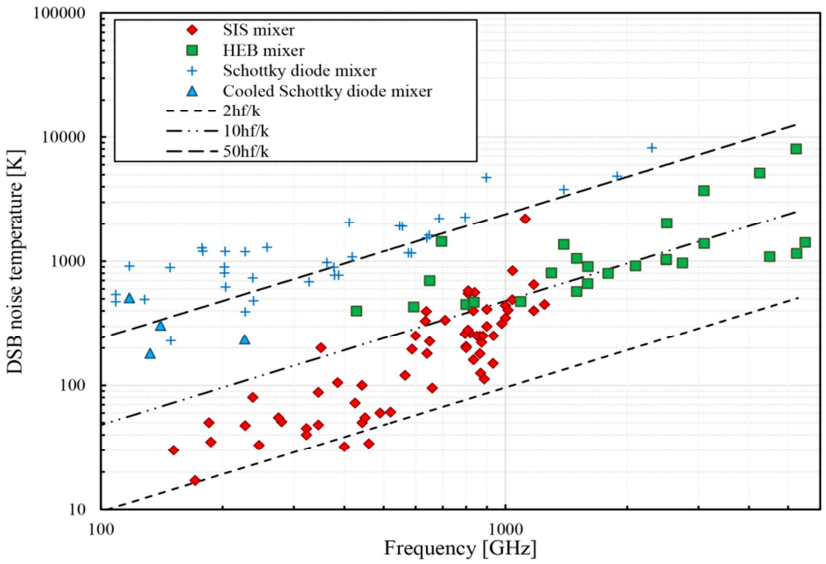

Figure 2: Comparison of noise temperature versus operating frequency of different mixer technologies plotted against multiples of the fundamental quantum noise floor, illustration from [12].

Ultimate noise performance in the frequency range from approximately 100 GHz to 1.2 THz is achieved with SIS mixers, as seen in Figure 2. Their working principle is based on a photon assisted, quasiparticle tunneling through an SIS junction and they can be operated close to the fundamental noise limit [10]. However, they obey an upper frequency limit, which is determined by twice the energy gap of the superconducting material in use. The most mature SIS technology is based on a Nb/Al-AlO_x/Nb trilayer, which limits the operation to approximately 1.4 THz. Beyond that frequency, the phonon-cooled HEB mixers based on a ultra-thin NbN film have proven to be generally the preferred technology.

In contrast to the SIS mixer and the Schottky diode, which employ a non-linear voltage-current characteristic to down-convert the signal, the frequency mixing in HEBs is based on a temperature modulation caused by the power of the beating signal of LO and RF and obeys, in theory, no upper frequency limit of operation. However, the loss introduced by the embedding circuitry will increase significantly with frequency and eventually deteriorate the noise performance of the receiver. The major challenge that is frequently faced with the operation of HEB devices is their rather small IF bandwidth at their lowest noise performance of approximately 3-4 GHz [13].

Besides the interest of radio astronomers in this frequency range, it also found applications in medical imaging, material analysis and research, defense and security applications [14] as well as in communication [15].

1.2 The niobium nitride superconductor

The contribution of NbN material to the advances in submillimeter and terahertz electronics is significant and led to the establishment of phonon-cooled HEB mixers with moderate IF bandwidth [16], utilizing its short intrinsic interaction times and relatively high T_C.
The existence of superconductivity above temperatures of 10 K was experimentally proven for the first time with the discovery of niobium nitride's superconducting transition at 16 K in 1941 [16]. Although its properties have been studied in detail over the last 6 decades, only few applications of NbN have evolved until the 80s [11]. The reason behind this was the competition with Nb and NbTi, which allowed for a more controlled fabrication process in a larger scale. In addition, NbN can crystallize into multiple phases whereas only the cubic NbN_{1-x} δ-phase, the tetragonal Nb_4N_{3x} γ-phase and the hexagonal Nb_4N_5 are superconducting at about 16 K, 12 K and 10 K, respectively [17], [18], [19], [20]. The crystal structure and the formation of aforementioned phases can be seen in Figure 3. The formation of the δ-phase with highest critical temperature is stable, according to the phase diagram, at temperatures above 1200 °C and for a N/Nb ratio of 1 and greater [21]. The need of such high temperatures to synthesize NbN was challenging and originally performed by the nitridation of Nb in a nitrogen rich atmosphere for up to 50 hours [22].

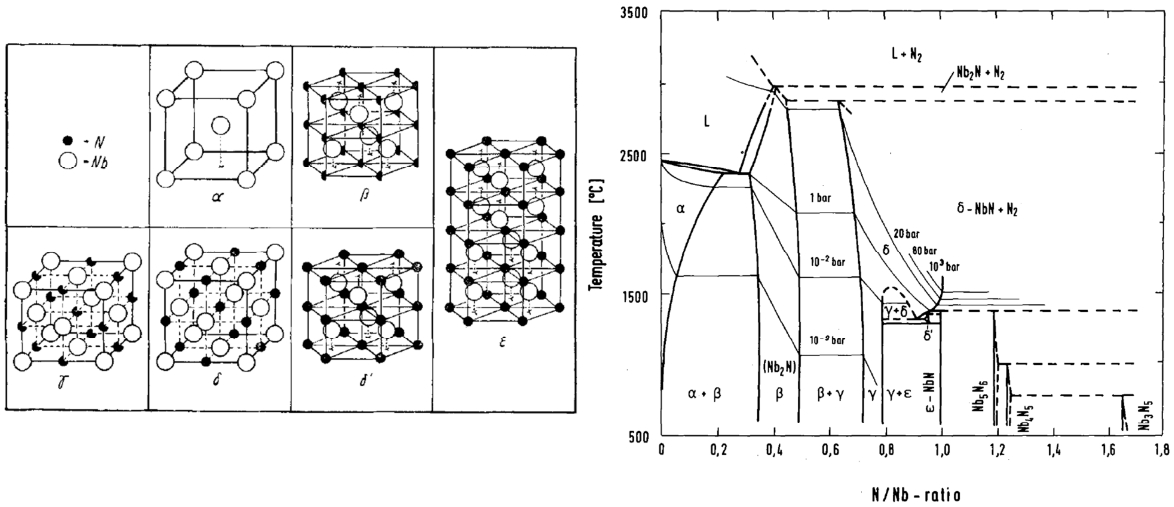

Figure 3: a) Crystal structure of the individual NbN phases [22] b) Phase diagram of NbN as a function of temperature and N/Nb ratio [21]

Extensive research on the synthesis of NbN thin films has been conducted since the discovery of its superconductivity as seen by the number of publications concerning this topic. This indicates the general interest for this material, not only for radio astronomical instruments. However, the suppression of NbN's superconducting properties when the film thickness is only several nanometers, as it is necessary to push the performance of phonon cooled HEB mixer, still represents a major technological challenge.

NbN thin films have found further employability in SIS junctions and mixers [23], [24], Superconducting Single Photon Detectors SSPD [25], superconducting IF circuitry, Superconducting Quantum Interference Devices (SQUID), Rapid Single Flux Quantum circuits (RSFQ) [26], kinetic inductance detectors (KID) and RF cavities.

1.3 Motivation

This thesis aims at the prospective improvement of IF bandwidth of phonon cooled HEB mixers with the consequence of making receivers more efficient for astronomical observations in the submillimeter and THz range. The performance of such devices is strongly linked to the superconducting properties of the NbN film and the substrate used to grow it onto. The improvement of the quality of the ultra-thin NbN films was achieved by employing a GaN buffer-layer which also provides a good acoustic match.

1.4 Thesis structure

The Chapter 2 describes the theory of hot electron bolometer mixers, specifically the phonon cooled HEB. Particular emphasis is put on the description of relaxation processes, responsible for the cooling of hot electrons and in consequence determining the IF bandwidth of the HEB.
In order to improve the performance of those devices, high quality and ultra-thin NbN films are required and its fabrication is addressed in Chapter 3. Superior superconducting and structural properties for NbN films grown onto an $Al_xGa_{1-x}N$ buffer-layer are presented and put into comparison with available NbN films.
In the chapter 4, the applicability of the GaN buffer-layer for the use in NbN HEBs is demonstrated in a simple mixer experiment at 180 GHz, focusing on the influence of buffer-layers on the mixer's IF bandwidth.
Chapter 5 contains concluding remarks and a short outlook of the thesis.

2
Hot Electron Bolometer

2.1 Working principle

A bolometer can essentially be regarded as a thermometer, which translates a change of the temperature into a measurable entity such as the resistance. As it is illustrated in Figure 4, the absorber is characterized by its heat capacity and a temperature-dependent resistance behavior and is connected via a thermal link with a colder heat reservoir usually of a constant bath temperature.

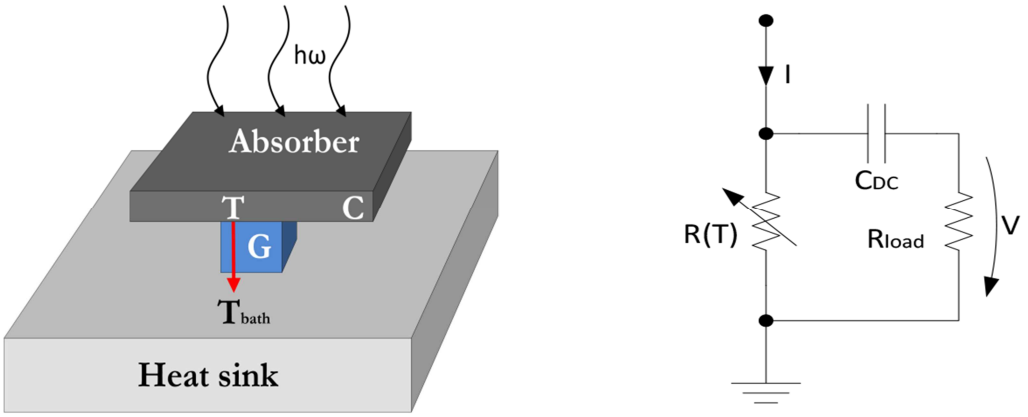

Figure 4: a) Schematic of bolometer consisting of the absorber, thermal link and a cold heat reservoir (heat sink) b) Electrical read-out circuitry for bolometers

Upon the absorption of incoming radiation, the temperature of the bolometer changes, which can physically be described by the thermal balance equation (1).

$$P = C\frac{dT}{dt} + G(T - T_{bath}) \tag{1}$$

Solving the heat balance equation upon steady radiation and after interruption yields the following temperature response:

Steady irradiation: $T(t) = T_{bath} + P/G$

Stopped radiation: $T(t) = T_{bath} + P/G \cdot e^{-\frac{t}{\tau}}$ and $\tau = C/G$

The characteristic response time τ describes the speed of the bolometer and is the ratio of the bolometer's heat capacity and thermal conductance G of the link to the underlying heat sink.
The read out can simply be performed by the circuitry presented in Figure 4b. The incoming radiation is repeatedly turn on and off by a chopper at a low modulation frequency ($\omega_{chop} \ll 1/\tau$) and causes the absorbed power and in consequence the resistance to change. The current biasing of the bolometer generates therefore an alternating voltage swing which is passed through the coupling capacitor and eventually read out across a load resistance. The responsivity of the bolometer is therefore also defined as voltage change per absorbed power $S_A = dV/dP\,[V/W]$ and is proportional to the dependence of resistance to temperature dR/dT of the material used as thermometer.

The HEB is based on a thin superconducting material with a typical resistance-temperature behavior as Figure 5a depicts. At the transition from the normal to the superconducting state, the resistance drops rapidly due to the strong dependence of the density of quasi-particles upon a change in temperature close to T_c which manifests in the high sensitivity.

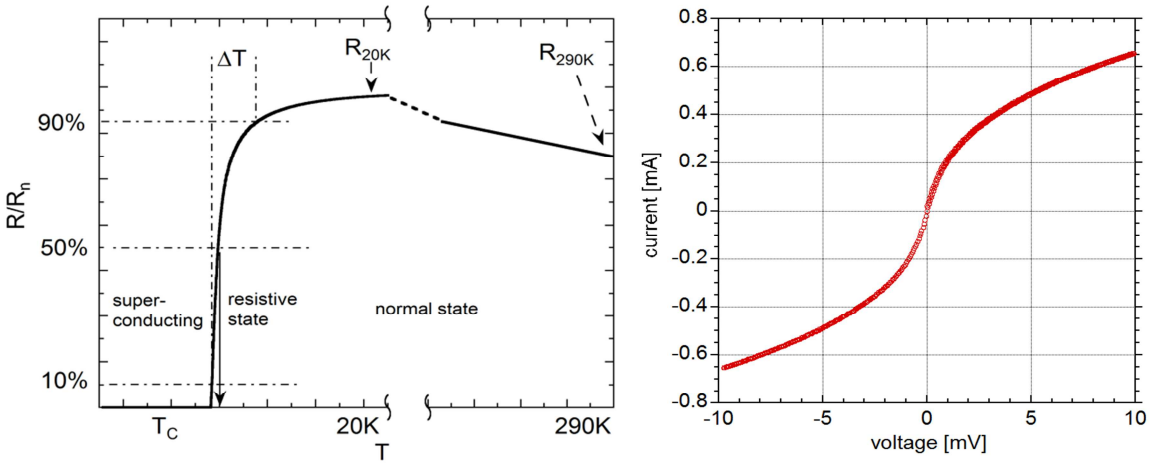

Figure 5: a) Resistance versus temperature behavior of an ultra-thin NbN film and the corresponding states. b) Typical IVC of a pumped HEB. The bridge is in the normal state, as indicated by the almost linear slope for high applied bias voltages.

In contrast to an ordinary bolometer, only electrons are heated and not the entire lattice. The term "hot electron" is used in the content of a thermal non-equilibrium of the electronic system and the lattice (phonons), originally found in semiconducting devices when applying high input power to them [27]. Under these circumstances, the rate of energy loss due to the lattice is smaller than the incoming power and results in the direct heating of carriers. This phenomenon has

also been observed in thin superconducting films in their resistive state and led to the development of the HEB [11].
Hot electron bolometers are operated in their resistive state, close to their critical temperature along with applied DC bias current as illustrated in Figure 6a. The time needed to thermalize electrons upon the absorption of a photon can be very short and is of the order of several picoseconds for NbN material [28], Figure 6b. The thermal link in a HEB can be considered as all processes that enable the hot electrons to exchange their energy to the surrounding heat sink. Thus electrons exchange thermal energy to the colder normal metal contact pads or the substrate, see Figure 6c,d.

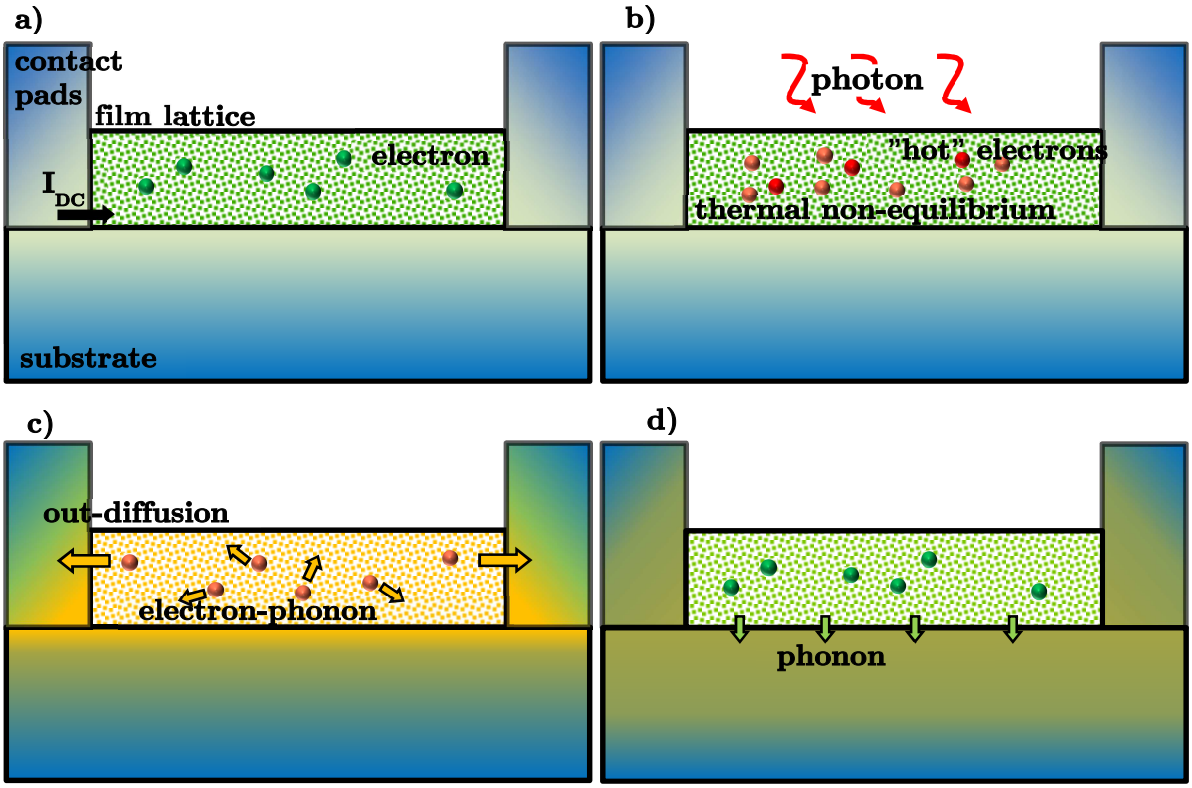

Figure 6: a) HEB bridge in the resistive state by current biasing b) The absorption of photons thermalizes electrons within a short time and leads to a thermal non-equilibrium between electrons and phonons c) Cooling of the electrons either by out-diffusion to the contact pads or energy exchange with the lattice d) Heat exchange between the film phonons and the substrate, also called phonon escape

The diffusive cooling is dominating when the thermal electron diffusion path is in the range of the lateral dimension of the bolometer so that electrons can directly out diffuse to the normal metal contact pads. For practical HEBs based on Nb material that is the case for bridge for approximately 40-70 nm for clean Nb films with diffusion constant $D = 1.6\,\mathrm{cm}^2/\mathrm{s}$ [29]. The diffusion length L_{diff} is calculated by $L_{diff} = \sqrt{D \cdot \tau_{e-ph}}$. The performance of such diffusion cooled devices turned out to be scattered because of the challenging fabrication on a nanometer scale, the inhomogeneity of the thin Nb layer itself and reliability issues with the quality of the contact pads due to oxidation and defects.
The second possibility for electrons to relax their energy is through the lattice. This process is dominating for disordered films in the dirty limit such as NbN. The

short electron-phonon interaction time of 12 ps in this material prospects short bolometer time constants, equivalent to an IF bandwidth of more than 15 GHz [30] if operated as a mixer. However, such high frequencies were never observed because of the fact that the excess energy of the lattice needs to be removed by the underlying substrate, which hinders the speed of the device. Moreover, the self-heating effect or electro-thermal feedback will affect the IF bandwidth as well. Another material that also exhibit short intrinsic electron-phonon and escape times is MgB_2 with T_c of 39 K, which has recently proven to be competitive to NbN material [31] in terms of the IF bandwidth.

2.2 Frequency mixing in HEBs

The mixing of RF signals in a HEB is fundamentally different from the down conversion based on a non-linear voltage-current characteristic as it is the case e.g. in SIS or Schottky mixers used at submillimeter and THz frequencies. By assuming two superimposed electrical signals with $E_{LO}(t) = A_{LO} \cdot \cos(\omega_{LO} t)$ and $E_{RF}(t) = A_{RF} \cdot \cos(\omega_{RF} t)$ across the bolometer, the absorbed power in the HEB can be written as Eq. (2), where α is the coupling efficiency.

$$P(t) \propto \alpha (E_{RF} + E_{LO})^2 + P_{DC} \tag{2}$$

Now, by inserting the RF and LO signal into Eq. (2) yields:

$$\begin{aligned} P(t) \propto \alpha \Bigg(& \frac{A_{LO}^2}{2} + \frac{A_{RF}^2}{2} + \frac{A_{LO}^2}{2}\cos(2\omega_{LO}t) + \frac{A_{RF}^2}{2}\cos(2\omega_{RF}t) \\ & + A_{LO}A_{RF}\cos\big((\omega_{LO} + \omega_{RF})t\big) + A_{LO}A_{RF}\cos\big((\omega_{LO} - \omega_{RF})t\big)\Bigg) + P_{DC} \end{aligned} \tag{3}$$

From Eq. (3) we can identify the generation of the frequency components $2\omega_{LO}$, $2\omega_{RF}$, $\omega_{LO}+\omega_{RF}$ as well as the difference frequency ω_{LO}-ω_{RF}, which is identical to the intermediate frequency. This frequency beating by means of absorbed power will only be observed if the temperature of the hot electrons was capable of following the fast change induced by the incoming radiation. In practice, the characteristic time is in the range of several tens of picoseconds which translate to a few GHz [28]. Thus, the time dependence of the temperature will only follow the $\cos(\omega_{LO}$-$\omega_{RF})$ term as in Eq. (4), which causes a change in the HEB's resistivity and, with applied DC bias, consequently generating the IF voltage across the bolometer.

$$P(t) \propto P_{DC} + \alpha \left(\underbrace{\frac{A_{LO}^2}{2} + \frac{A_{RF}^2}{2} + A_{LO}A_{RF}\cos(|\omega_{LO} - \omega_{RF}|t)}_{down-converted} \right) \tag{4}$$

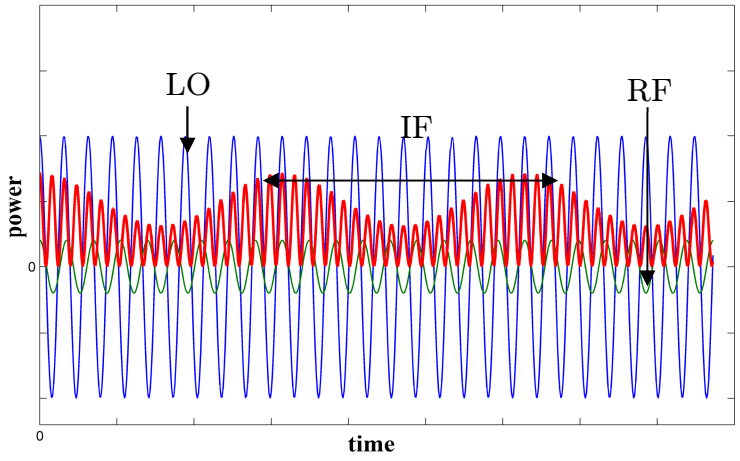

Figure 7: Illustration of the thermal modulation across the HEB bridge with the difference frequency $|\omega_{LO} - \omega_{RF}|$. The levels are not in proportion.

Figure 7 illustrates the power dissipated in the bolometer, the absorption of superimposed LO and RF signal yields a thermal modulation with the difference frequency ω_{IF}.
The absorption of photons is not dependent on the superconducting properties such as energy gap or in consequence the critical temperature of the superconducting material in use since it is operated in its resistive state, thus theoretically it does not have an upper frequency limit of operation as in contrast to the competing SIS mixer technology with highest frequency of operation limited to twice the energy gap of the superconductor that the SIS junctions is constituting of.

2.3 IF bandwidth in phonon-cooled HEBs

As described earlier, the resulting IF bandwidth can be associated with the cooling rate of hot electrons either by the diffusion or the phonon cooling. In practice the phonon-cooled NbN HEB is the dominating technology and only the investigation of afore mentioned phonon cooling channel will be described here in detail.

2.3.1 IF bandwidth estimation

The first attempt to model the gain bandwidth of HEBs dates back to 1987 and was based on heat balance equations where electrons and phonons were treated as having uniform but different temperatures, also known as the 2-T model [32]. The following set of equations was obtained by linearizing the 2-T model at temperatures close to T_C, and assuming a uniform temperature distribution across the bolometer bridge. The transfer function $\Psi(\omega)$ contains three characteristic

time constants which themselves depend upon the electron-phonon interaction time τ_{e-ph} , escape time of phonons τ_{esc} and the ratio of specific heat capacities of electrons c_e and phonons c_{ph}.

$$\Psi(\omega) = \frac{(1 + i\omega\tau_1)(1 + i\omega\tau_2)}{1 + i\omega\tau_3} \tag{5}$$

And the three time constants being:

$$\tau_1^{-1}, \tau_2^{-1} = \frac{\Omega}{2}\left(1 \mp \sqrt{1 - \frac{4\tau_{e-ph}^{-1}\tau_{esc}^{-1}}{\Omega^2}}\right) \tag{6}$$

$$\Omega = \left(1 + \frac{c_e}{c_{ph}}\right) \cdot \tau_{e-ph}^{-1} + \tau_{esc}^{-1}$$

$$\tau_3^{-1}, = \frac{c_e}{c_{ph}}\tau_{e-ph}^{-1} + \tau_{esc}^{-1} \tag{7}$$

Applying Eq. (5) and using typical properties of thin NbN films, then the transfer function can be plotted over frequency. The 3-dB roll off or in decimal scale 0.5 is the figure-of-merit for determining the IF bandwidth of the HEB mixer.

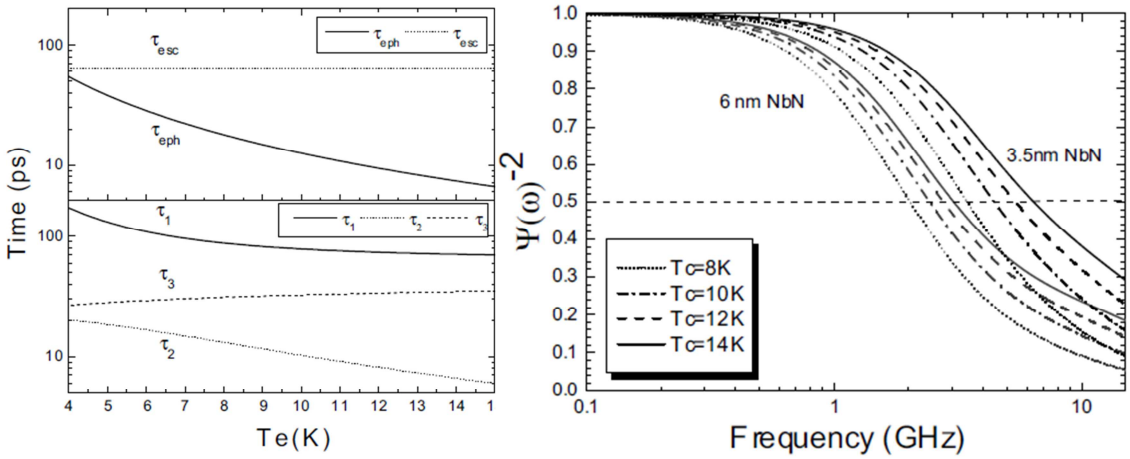

Figure 8: a) The characteristic time constants are plotted over electron temperature. b) The transfer function which was derived from the time constants versus frequency for different critical temperatures and film thicknesses. Recreated from [33].

Figure 8 depicts the dependence of the characteristic time constants versus electron temperature. It can be seen that by increasing the temperature, the electron-phonon interaction time is reduced, whereas the escape time does not depend on temperature. Moreover, by reducing the film thickness while maintaining high critical temperature leads theoretically to the highest IF bandwidth.

2.3.2 Electron-phonon system

The electron-phonon system describes the interaction process taking place between the electrons and the lattice. In the case of a pure metal and for temperatures much lower than the Debye temperature $T \ll \Theta$, electrons are solely scattered on phonons at small angles and at a rate linearly proportional to the temperature. However, in the presence of impurities and for film thicknesses smaller than the phonon mean free path, the interaction rate between electrons and phonons can substantially differ from the clean case and bulk materials [34].

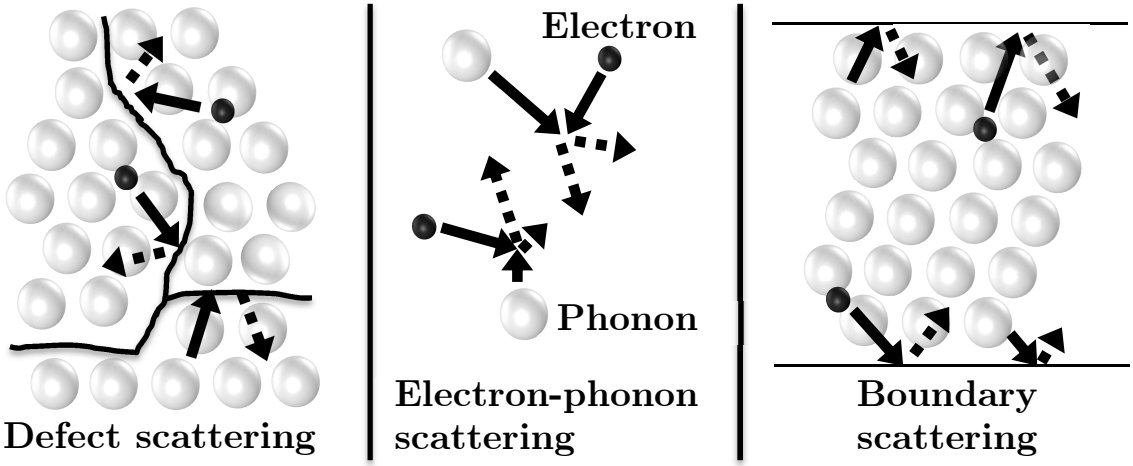

Figure 9: Scattering mechanisms in thin films

The Figure 9 illustrates the most dominant scatter mechanisms found in thin superconducting films. The interaction on defects and electron-phonon scattering will be described more detailed below. The scattering of phonons on boundaries is dominating over the collision with other phonons because the phonon mean free path is longer than the smallest dimension i.e. the film thickness. The phonon-phonon interaction will be treated in the following subchapter "Phonon escape".

The product of phonon wave number and electron mean free path $q_T l_e$ defines the dominating scatter mechanism. In the impure or "dirty" limit for $q_T l_e \ll 1$, electrons will additionally experience inelastic as well as elastic electron-impurity scattering depending on the type of scatterer. Vibrating scatterers such as defects or boundaries move along the same way as the lattice or host atoms whereas non-vibrating impurities move independently [35]. In the case of strong disorder $q_T l_E \ll 1$ the electron-phonon interaction rate can be described by

$$\tau_{e-ph}^{-1} = \underbrace{\frac{\pi^4 T^4 l_e}{5\rho_F^2}\left[\frac{\beta_l}{v_l^3} + (1 - l/L)\cdot\frac{3\beta_t}{2v_t^3}\right]}_{longitudinal\ phonons} + \underbrace{\frac{\pi^2 T^2}{2\rho_F^2 L}\left[\frac{\beta_l}{v_l} + (1 - l/L)\cdot\frac{2\beta_t}{v_t}\right]}_{transverse\ phonons} \tag{8}$$

Where L is the electron mean free path in respect to the non-vibrating potential and β is the kinetic constant of the electron-phonon interaction defined as:

$$\beta_{l,t} = \left(\frac{2}{3}\epsilon_F\right)^2 \cdot \frac{N(0)}{2\rho_m v_{l,t}^2}$$

With ϵ_F the Fermi energy, N(0) the two spin density of electron states, ρ_m the density of the metal, $v_{l,t}$ the longitudinal and transverse sound velocity, respectively [36] [37]. By analyzing Eq. (8) we can see that very large L, as in the case of only vibrating impurities, the interaction with transverse phonons is negligible and the T^4 temperature dependence is dominating. However, this has only been observed for few elements such as thin Bi films [38]. In practice, the squared temperature dependence is found much more widely and points towards the dominating scattering mechanism due to non-vibrating impurities with transverse phonons [36] .

In the temperature range of interest (4.2 to 15K) NbN can be considered as a disordered material with $q_T l_E$ in the range of approximately 0.05-0.16 when using v_m=5000m/s (average sound velocity) [26-29] and the electron mean free path l_e=0.4nm [39]. Therefore, assuming the dirty limit and the dominating interaction with transverse phonons [40] Eq. (8) simplifies to

$$\tau_{e-ph}^{-1} = \frac{9}{8} B T^2 F_t(q_t l_e) \cdot v_f / l_e \tag{9}$$

$$B \approx \frac{4\pi^2 k_B^2 \beta_t}{3\epsilon_F \rho_F v_t}$$

Then we can deduce the following dependencies of the electron-phonon rate.

$$\tau_{e-ph}^{-1} \propto \epsilon_F, N(0), T^2, l_e^{-1}, v_t^{-3} \tag{10}$$

By modifying the stoichiometry of the NbN compound we are capable of influencing the electron-phonon interaction rate already during the growth of the films.

Experimental studies support the presence of the dominating transverse phonon scattering process in thin NbN films by identifying a $T^{-1.6}$ temperature dependence [41]. Hence, rising the operating temperature and in turn the critical transition temperature to the superconducting state, shorter electron-phonon interaction times should be achieved. This can be accomplished by promoting the growth of single crystal films with improved superconducting properties. However, the Fermi energy ϵ_F, density of states $N(0)$ and electron mean free path l_e will also be substantially different from poly-crystalline to epitaxially grown films. The believe that highly disordered poly-crystalline films with shorter electron mean free path yield a higher electron-phonon interaction rate compared to single crystal films is counteracted by their reduced density of states and fermi energy [42] as it also can be qualitatively explained by a crude model [43].

2.3.3 Phonon escape

After the relaxation of non-equilibrium quasi-particles on phonons, their energy needs to be removed by another, cooler heat reservoir. The processes being involved in the relaxation of heated film phonons is called phonon escape and is affected by manifold sub processes as illustrated in Figure 10.

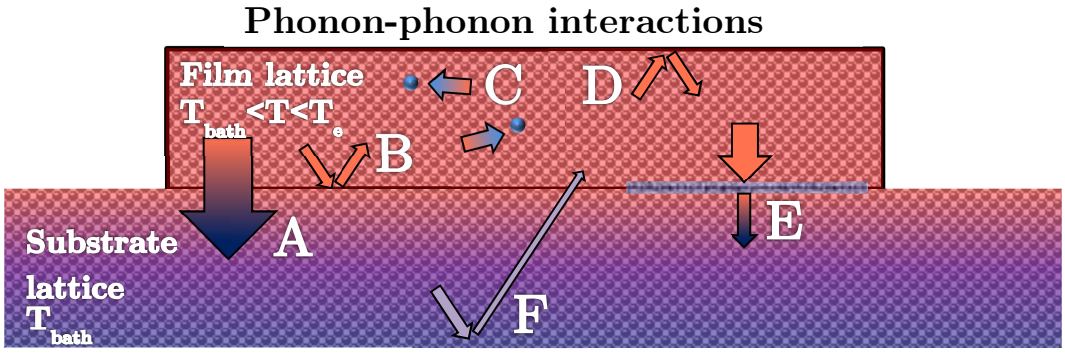

Figure 10: The arrows depict energy transfer processes which play a role in the phonon escape in thin films and own characteristic times. A: Escape of phonons to the lattice τ_{esc}; B: Acoustic mismatch of film phonons and substrate phonons leads to reduced phonon transmissivity α; C: Backflow of energy from phonons to electrons τ_{ph-e} ; D: Reduced phonon heat conductivity due to boundaries; E: Reduced heat transfer due to defects at the interface; F: Backflow of energy from the substrate phonons to film phonons, phonon trapping in substrates if it only has limited dimensions

The main contributor to the cooling of film phonons is the exchange of energy to the cooler underlying lattice of the substrate which is held at the bath temperature, also seen as process (A) in Figure 10. However, the rate of which phonons can escape is in practice hindered by additional interaction processes such as phonon reflection due to acoustic mismatch (B), defects at the interface (E) and boundaries (D,E,F) as well as the backflow of energy from the film lattice to its electrons (C). In order to enhance the overall phonon escape, all factors will be addressed and desirable superconducting properties for the NbN film derived.

A – Phonon escape

In the limit where the phonon mean free path is determined by the lateral boundary conditions i.e. the film thickness $d \geq \Lambda$ and for specular scattering at the film/substrate interface, the escape time can be approximated by Eq. (11).

$$\tau_{esc} = \frac{4d}{\alpha v_m} \tag{11}$$

Where α is the phonon transmissivity and v_m the mean acoustic velocity. In consequence the escape time is proportional to the film thickness and should therefore be kept as low as the suppression of superconductivity does not become overwhelming, i.e. in the range of a few nanometer [44]. The mean velocity of sound can be calculated from the superimposed longitudinal and transverse acoustic velocities according to Eq. (12).

$$v_m = \frac{1}{3}\left(\frac{1}{v_l^3} + \frac{2}{v_t^3}\right)^{-1/3} \tag{12}$$

The sound velocities of NbN can be determined by measuring its elastic constants. This has been done in several studies [45] [46] [47] [48] with small discrepancies and the mean value of 4900m/s shall be used throughout this work.
In practice however, theoretical predictions for the escape time following Eq. (11) usually fail because the phonon transmissivity α can be as low as 10 % for certain substrates which are acoustically mismatched to the NbN film. The first study on acoustic matching of thin films has been done by Little in 1959 [49] and based on these results Kaplan developed a more rigorous theory, in particular treating the acoustic matching of superconducting films to substrates [50].

B – Acoustic matching

The acoustic mismatch theory is based on the calculation of transmission coefficients of both longitudinal and transverse phonons incident at the interface between film and substrate by employing Snell's law. Several assumptions were made such as semi-infinite media and perfect planar contact and it was concluded that not only transmission coefficients depend on the angle of incident also total reflection of phonons can occur at the interface. Figure 11 illustrates the dependence of longitudinal transmission coefficient η_l on the ratios of acoustic velocities and densities of film and substrate, respectively. It can be seen that substantial acoustic matching is achieved for high density substrates with low acoustic velocity relative to the film. Moreover, the Figure 11 contains marker which illustrate the performance of buffer-layers and substrates to match to NbN films.

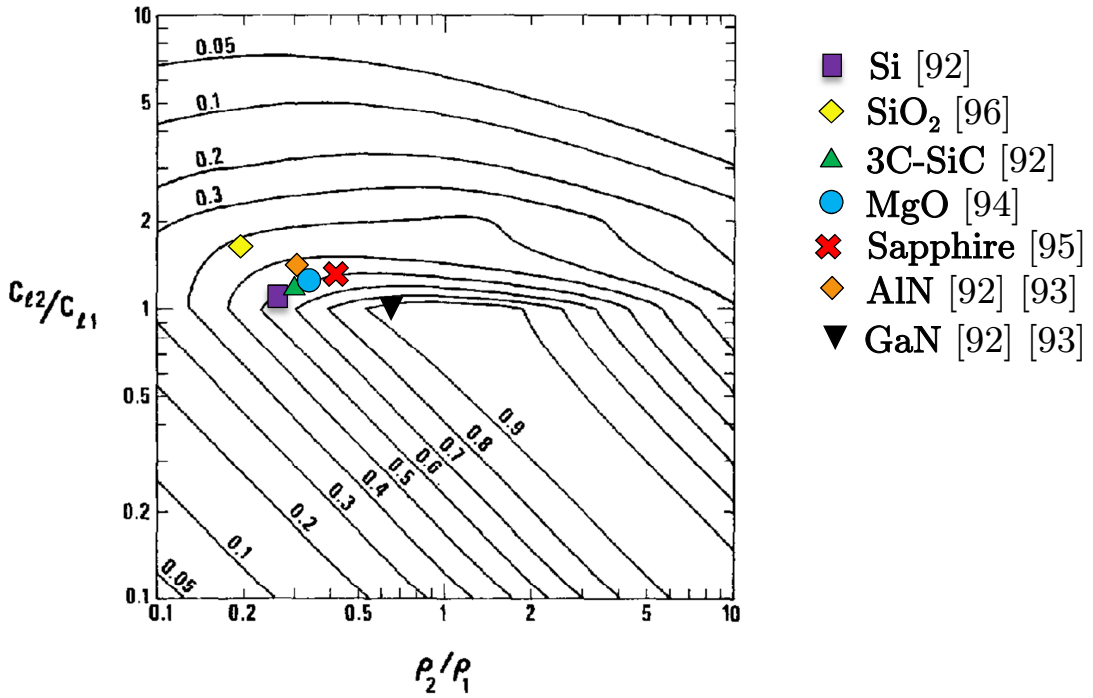

Figure 11: The contour of the longitudinal transmission coefficient is plotted in respect to the ratio of longitudinal acoustic velocities c_{l2}/c_{l1} and the densities ρ_{l2}/ρ_{l1} of substrate (2) and film (1), respectively. The markers indicate the performance of available substrates to match to NbN. The data used to calculate the transmission coefficients was obtained from the listed references.

Commonly used insulating substrates for NbN that promote the epitaxial growth are MgO [44], 3C-SiC [51] [52] and r-plane sapphire [53] exhibit poor acoustic match to NbN which in turn leads to the limited IF bandwidth. In contrast, GaN with its relatively high density compared to the other substrates may be a promising material for prospective enhancement of the phonon escape rate and motivates its further investigation in the frame of this work.

C – Backflow of phonons to electrons

The inverse process of relaxation of electrons to the lattice is the energy backflow from the lattice to colder electrons. In the frame of the two-temperature model (2-T model), first introduced by Kaganov [54], the heat balance equations can be linearized close to the critical temperature of the superconductor and is dependent on the heat capacity of electrons C_e and phonons C_{ph}, respectively. The earlier described complex relaxation of electrons to phonons is directly linked to the ratio of heat capacities according Eq. (13)

$$\tau_{ph-e} = \tau_{e-ph} \cdot C_{ph}/C_e \tag{13}$$

In order to prevent or decelerate the relaxation of the heated lattice to the electrons with the characteristic rate τ_{ph-e} the ratio of C_{ph}/C_e should be

maximized. At low temperatures the specific heat capacities can be expressed by Eq. (14) and (15) and omit different temperature dependencies.

$$c_{ph} = \frac{12\pi^4}{5} Nk \left(\frac{T}{\theta}\right)^3 \tag{14}$$

$$c_e = \gamma T \tag{15}$$

With N density of atoms, Θ the Debye temperature and γ the Sommerfeld constant ($\approx 1.85 \cdot 10^{-4} J/cm^3$ for NbN). Thus, the ratio C_{ph}/C_e follows a quadratic temperature dependence, and it can be stated that rising the temperature of the HEB, i.e. increasing the film's critical temperature will lead to a reduced phonon-electron energy backflow.

D – Phonon trapping due to boundaries

The contribution of the film phonons to the removal of heat plays only a minor role in ultrathin films and low temperatures since the phonon mean free path Λ_{film} is significantly shortened by the boundaries, i.e. the film thickness. The thermal conductivity due to phonons k_{ph} can be calculated by Eq. (16) according to [55].

$$k_{ph} = \frac{1}{3} c_{ph} v_m \Lambda_{ph} \tag{16}$$

E – Reduction of phonon escape due to interface defects

The calculations of phonon transmissivity by Little and Kaplan are based on an ideal film-to-substrate interface which is hardly present in practice [49], [50]. The impact of defects at the interface of film and substrate was studied in detail for epitaxial Si/Ge layer [56] and reveal some general dependencies which shall be transferred to the interface of NbN film and substrates.

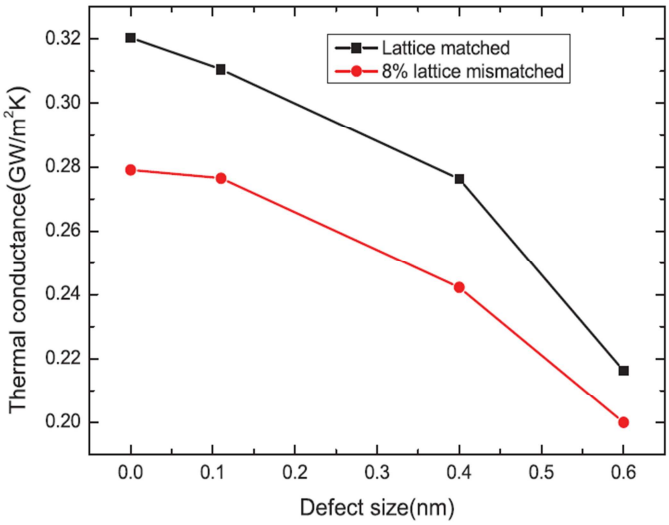

Figure 12: Thermal conductance versus defect size at the interface of Si and Ge for the lattice matched and slightly mismatched case. Reproduced from [56].

The thermal conductance in Figure 12 is directly related to the phonon transmissivity across the interface and decreases rapidly for increasing defect size. Introducing an additional alloyed layer at the interface has shown to reduce the thermal conductance proportionally to the layer thickness. The effect of lattice mismatch, however, is not as severe as defects such as stress, atomic reconstruction or species mixing. Applying these observations made on the Si/Ge interface [56] then the phonon transmissivity at the NbN/substrate interface can be maximized by employing a lattice matched buffer-layer which should be thermally stable to prevent interdiffusion during the deposition at elevated temperatures. Moreover, silicon and other substrates tend to build up a native oxide layer at their surface which, if not removed prior to the growth of NbN, will also hinder the escape of phonons.

F – Backflow of energy from the substrate to the film

The flow of heat from the substrate backwards to the film is not well understood but may additionally reduce the phonon cooling rate. The thermal conductivity of the substrate is mainly governed by the transport through phonons, however, for sufficiently thin substrates $d \leq \Lambda$ the conductivity is significantly reduced as seen from Eq. (16) and phonons can be trapped inside the substrate resulting in a rise of the bath temperatures. This effect will only be present for large bolometer sizes and thin substrates but may play a role for waveguide based HEBs operating at several THz which requires substrate thicknesses of only a few micrometers to not disturb the electrical fields excessively.

2.4 Remarks on the improvement of IF bandwidth

The relaxation process of hot electrons is manifold and thus all involved interaction mechanisms need to be considered in order to achieve a significant overall improvement of HEB's IF bandwidth. Increasing the temperature of electrons, i.e. increasing the critical temperature of the film will increase the heat capacity ratio C_{ph}/C_e and therefore lowers the electron-phonon time. This is in the favor of the overall mixer time constant. However, further enhancement of electron-phonon interaction will not necessarily lead to faster HEBs since the phonon escape to the substrate becomes the limiting time constant. By reducing the thickness of the film, the escape rate will be increased, however superconductivity will be dramatically suppressed when approaching film thicknesses of 3-4 nm as illustrated in Figure 13.

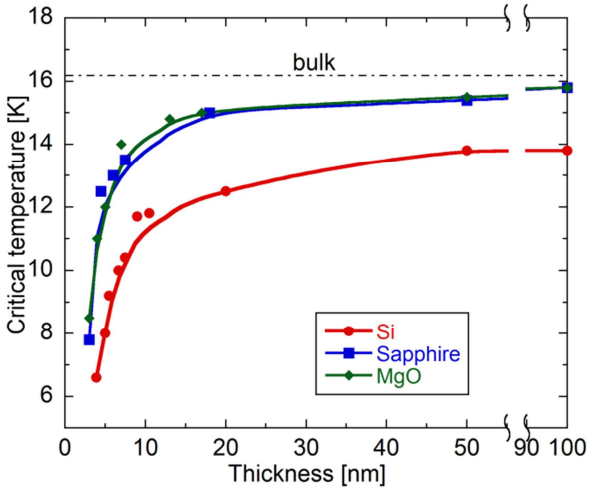

Figure 13: The suppression of superconductivity versus film thickness for different substrates. MgO [44] and sapphire substrate [53] yield single crystal films, whereas NbN deposited on silicon substrates have lower T_c due to the greater lattice mismatch [13], [57]

Following Eq. (11) a theoretical escape time of 4-5 ps could be achieved for a 5 nm thin NbN film exhibiting a perfect interface to an acoustically matched substrate. However, measured escape times for NbN ultrathin films are usually in the range of 30-50 ps [30] [41] and yield the limited IF bandwidth of only a few GHz. Thus, the acoustic matching of NbN to the substrate remains a major challenge and has not been achieved with commonly used substrates such as Si, MgO, sapphire or SiC, see Figure 11. Moreover, the film-to-substrate interface should be given special attention, e.g. applying sufficient cleaning of the substrate surface prior deposition of NbN as well as running a deposition process preferably at low temperatures to reduce impurities and interdiffusion from light elements from the substrate to the NbN film. Additional requirements on the substrate are chemical inertness and mechanical robustness to ease the application in practical waveguide-based HEB mixers.

3
Ultra-thin NbN fabrication

3.1 Thin film deposition techniques

The δ-phase of NbN is according to the phase diagram in Figure 3 only stable at temperatures above 1200 °C and is, in addition to it, sensitive to the ratio of N/Nb. Originally, NbN has been synthesized by the nitrification of Nb powders at high temperatures which was achieved in a furnace or by heating the sample with excessive RF power [22], [21]. It was found that the nitridation was supported by increasing the nitrogen pressure to several MPa, where Nb undergoes the following phase transitions [58]:

$$Nb \rightarrow \alpha - Nb(N) \rightarrow \beta - Nb_2N_{1\pm x} \rightarrow \gamma - Nb_4N_{3\pm x} \rightarrow \delta - NbN_{1\pm x}$$

With the continuous progress in thin film deposition techniques, it was soon feasible to fabricate NbN also with chemical deposition techniques such as the High Temperature Chemical Vapor Deposition (HTCVD) [59] or through a chemical solution polymer assisted deposition on SrTiO3 substrate [60].
In addition to that, many more techniques have been employed to successfully deposit NbN thin films such as pulse laser annealing [61], the pulse laser deposition technique [62], molecular beam epitaxy (MBE) [63] or the atomic layer deposition (ALD) [64]. Despite the numerous process technologies of growing NbN thin films, the DC magnetron sputtering from a pure Nb target in a reactive argon-nitrogen atmosphere became widely accepted as the deposition techniques of choice, particularly for growing ultra-thin films used for e.g. HEBs or SSPDs.
The Chapter 3.2 will describe the DC magnetron sputtering technique for growing ultra-thin NbN films in detail.

3.2 Reactive DC magnetron sputtering of NbN

DC magnetron sputtering belongs to the physical vapor deposition techniques (PVD) and utilizes a high-purity metal source (target) which is bombarded with ions of a noble gas. The energy of the sputtered atoms is initially in the range of several eV [65], [66] which is equivalent to a temperature of a few thousand Kelvin. Even though the arriving atoms lost part of their kinetic energy due to collisions until they reach the substrate surface, they are still in thermodynamic non-equilibrium, which makes the formation of the desired δ-phase of NbN possible.
Magnetron sputtering is somewhat different from normal sputtering since it confines the plasma close to the target surface. Magnetic fields are formed in such a way that electrons are trapped and the plasma is intensified, which itself is responsible for the eventual sputtering of the target material. It can be distinguished between the unbalanced and balanced magnetron configuration. The latter gives a better confinement of the plasma close to the target, whereas the unbalanced design exposes the substrate to more direct ion bombardment due to less plasma confinement. Depending on the process pressure, the sputtered atoms experience a ballistic trajectory (low pressure, long mean free path) or are scattered (high pressure, mean free path shorter than target-to-substrate distance) on their way to the substrate.
Reactive magnetron sputtering in addition, introduces a reactive gas which reacts and forms compounds with the sputtered material. Those are not only limited to conductive compounds and also insulating materials can be synthesized. This requires, however, a RF magnetron power source in order to not insulate or poison the target with unwanted arcing as a consequence. During reactive sputtering, the formation of the compound can take place at the target surface, in between the target and the substrate or the substrate surface.
The increased complexity of this deposition method requires the careful adjustment of numerous process parameters. In Table 1, the most important ones are listed. The stoichiometry of the NbN compound is crucial for achieving good superconducting properties. By changing the ratio N/Nb, the stoichiometry can effectively be modified. Adjustment of the sputter rate of Nb can directly be achieved by changing the magnetron power. Indirect ways to increase this rate is to lower the process pressure and thus increasing the mean free path of the sputtered niobium, however, there is a competing process present when the pressure is lowered. Due to the low fraction of ions close to the target surface the sputter effect is decreased as well as plasma instabilities and ignition problems could occur. The adjustment of nitrogen's partial pressure is more obvious and easier way to control rather than the adjustment of Nb sputter rate. Additional RF biasing of the substrate holder may influence the deposition rate but not the sputter rate due to sputtering from the substrate by accelerated ions.

Table 1: Relevant process parameters for the deposition of NbN thin films.

	Process parameter	Access / adjustability	affects NbN stoichiometry
Prior deposition	Substrate cleaning	very good	-
	Target conditioning	good	-
	Base pressure	moderate	-
Sputtering	Magnetron power	good	+++
	RF bias	optional	-
	Total pressure	very good	++
	Partial pressure Ar/N_2	very good	+++
	Substrate heating	optional	+
	Deposition time	very good	-
	Target-substrate distance	Poor	+
Post deposition	Annealing (T, t, gas)	poor - good	+
	Cooling rate	poor	-
	Storage	good	-

The aforementioned process parameters in interaction with one other need to be optimized in order to achieve NbN films with high quality. In Figure 14, such an optimization procedure is illustrated. The optimal range of nitrogen and argon partial pressure is particularly narrowed for films with good superconducting properties, i.e. high critical temperature and narrow transition width. This optimal range, however, shifts for different total pressure or actual target erosion. This has also been observed by Wang and Capone [67], [65].

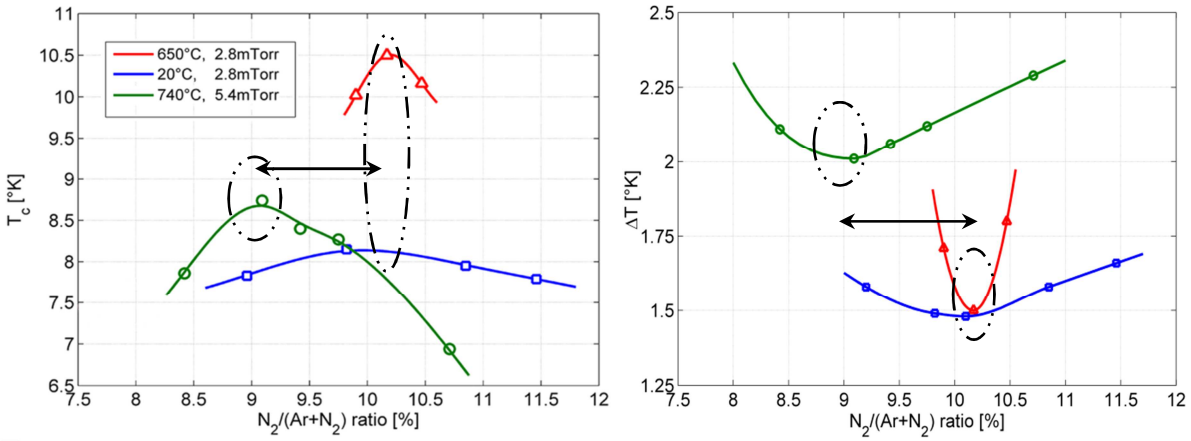

Figure 14: The optimal nitrogen partial pressure is dependent on total pressure, the thickness of the hot deposited films is 5nm and 7nm for the ambient temperature growth, this explains the reduced transition width compared to the thinner but hot deposited films.

The influence of substrate heating has been investigated and shows an increasing critical temperature of the deposited films if the substrate holder was heated up to approximately 650 °C for silicon substrates, as illustrated in Figure 15. It is understood that the mobility of arriving Nb atoms at the substrate surface is significantly increased by the additional thermal energy and leads to more ordered

films with fewer defects, as the increasing RRR is supporting this. With further increases of the substrate temperature, however, the RRR decays rapidly as well as the Tc of the film is lowered as illustrated in Figure 15. This can be associated with the incorporation of impurities in the film's lattice by outgassing of elements inside the vacuum chamber.

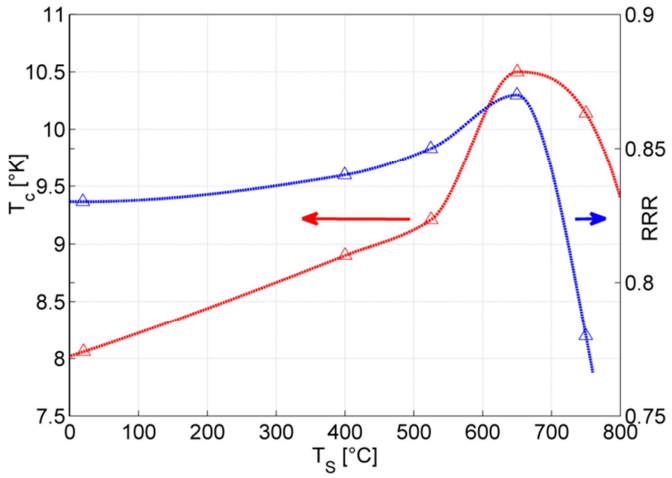

Figure 15: Critical temperature and RRR as a function of substrate holder temperature. The critical temperature of the 5 nm thin NbN film on Si increases up to 10.5 K at a substrate holder temperature of 650°C.

It can be concluded, that the optimization of process parameters in a reactive DC magnetron sputtering tool for the ultra-thin film deposition of NbN is manifold but provides eventually high quality films with high uniformity and repeatability. Particular importance needs to be given the adjustment of the partial pressure of nitrogen and argon as they mostly affect the film stoichiometry. Substrate heating has also proven to be essential for good superconducting properties of polycrystalline NbN films.

3.3 Surface analysis of NbN

During the last years it has increasingly been reported on the influence of the contact interface on the performance of phonon cooled HEB mixers [68], [69], [70]. A crucial process step in the fabrication of HEBs is the definition of the bolometer area by placing contact pads of a normal metal, usually a thin Ti layer for adhesion followed by a thicker Au layer [71]. Therefore, bad quality of the interface between NbN and the contact pads will lead to additional series resistance and in turn deteriorates the noise performance of the HEB mixer [71]. After the deposition of the NbN film, the exposure to ambient air will inevitably cause its surface to oxidize. The removal of this thin layer by Ar^+ etching [71], [72]

prior the deposition of contact pads has proven to be sensitive as it easily causes the NbN film to degrade.

There is only little understanding of the nature of the oxide that forms at the surface of ultra-thin NbN films. Frankenthal, Gallagher and Ermolieff have investigated the thermal oxidation of NbN surfaces of relatively thick layers (up to 1500 nm [73]) and bulk material [74], [75] and concluded the formation of mainly Nb_2O_5 as it is also found on bare Nb surfaces. Although for temperatures below 450 °C also amorphous or polycrystalline NbO_x has been identified.

Employing surface sensitive methods such as X-ray photoelectron spectroscopy (XRD) and reflective electron energy loss spectroscopy (REELS), the oxide state has been identified from the energy shift of NbO_x to Nb according to $x = 1.03 \cdot \Delta E$ [76]. In fact the in [Paper B] investigated NbN ultra-thin films exhibit an energy shift of 4 eV to the Nb 3p3/2 peak which clearly identifies the presence of NbO_2 at the surface. To the contrary, on the pure Nb film the energy shift of 4.9 eV was detected which corresponds to the widely observed Nb_2O_5.

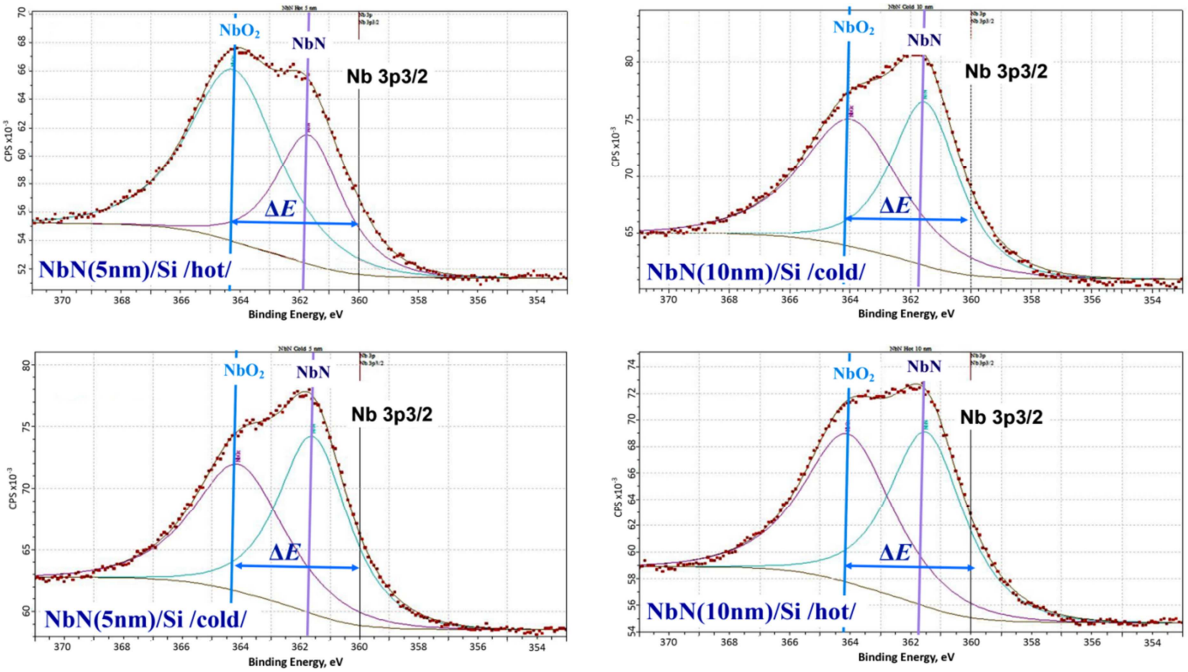

Figure 16: XPS spectra superimposed by the peaks of Nb 3p3/2, NbN and NbO_2. The absence of the Nb 3p3/2 peak in all films despite different growth conditions and thickness and the alignment of all NbN peaks is evidence of the identical film composition, reproduced from [Paper B].

The NbO_2 oxide that is formed at the surface of ultra-thin NbN in ambient atmospheres has a semiconductor-like nature as in contrast to the insulating Nb_2O_5 [76].

3.4 NbN growth on buffer-layers

Crystalline substrates with lattice constant close to the material to be deposited can promote the alignment of the growing material along its own crystal orientation. Hetero-epitaxy describes this process: two different materials are present nonetheless their crystal lattices match. In this case the deposited material grows as a single crystal and exhibits properties similar to, as if it was grown in bulk thickness. Small lattice mismatch will result in stress or elastic deformation in the film lattice. The δ-phase NbN is arranged in a face centered (fcc) cubic crystal with lattice constant of a=4.46 Å for single crystal thin films with highest reported T_c [67].
The Table 2 presents possible substrates and buffer-layer that have been used for the deposition of NbN ultra-thin films. It can be noted that substrates with high lattice mismatch yield only disordered and polycrystalline NbN with relatively poor superconducting properties. MgO, 3C-SiC and sapphire substrates have commonly been employed to promote the high quality growth of mono crystalline ultra-thin NbN films to overcome the suppression of the superconducting properties with reduction in thickness.

Table 2: Buffer-layer and substrates used for the deposition of ultra-thin NbN.

Buffer-layer/ Substrate	Lattice mismatch	Structure	NbN structural property	Reference
Si	+ 18%	diamond	polycrystalline	[57], [Paper A]
Si_3N_4	+ 41%	hexagonal	polycrystalline	[77] [78]
SiO_2	n.a.	amorphous	polycrystalline	[77]
Quartz	+ 9%	hexagonal	polycrystalline	[79]
MgO	- 6%	polycrystalline/ rock salt	single crystal	[44], [80]
Al_2O_3	+ 6%	hexagonal	single crystal	[53]
3C-SiC	- 2%	rock salt	single crystal	[51], [52]
GaAs	+ 21%	zinc blende	polycrystalline	[81]
Nb_5N_6	n.a.	polycrystalline	polycrystalline	[82]
TiN	- 5%	polycrystalline/ rock salt	polycrystalline	[83]
AlN	-1 %	polycrystalline	polycrystalline	[84]
$Al_xGa_{1-x}N$	-1% to +1%	wurtzite	single crystal	[Paper A]

Moreover, it has recently been shown the possibility to utilize a hexagonal crystal structure to align the cubic NbN crystal in its (111)-orientation, as it is illustrated in the Figure 17 [Paper A].

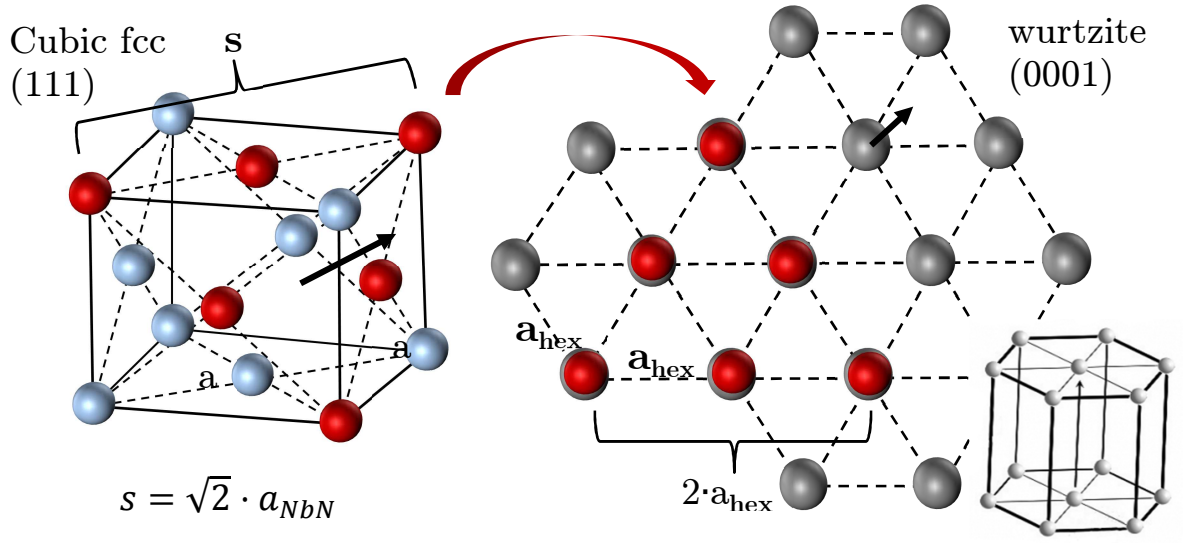

Figure 17: Alignment of the cubic fcc (111) orientation into the (0001) orientation of a hexagonal lattice.

The lattice mismatch of the substrate is crucial for the structural properties of the NbN film and in consequence for its superconducting properties. Thus, substrates with relatively large lattice mismatch or with amorphous structure will not support the single crystal growth of NbN, resulting in a T_c of not exceeding 10.5 K for a 5 nm thin film deposited onto Si or GaAs, see Figure 18.

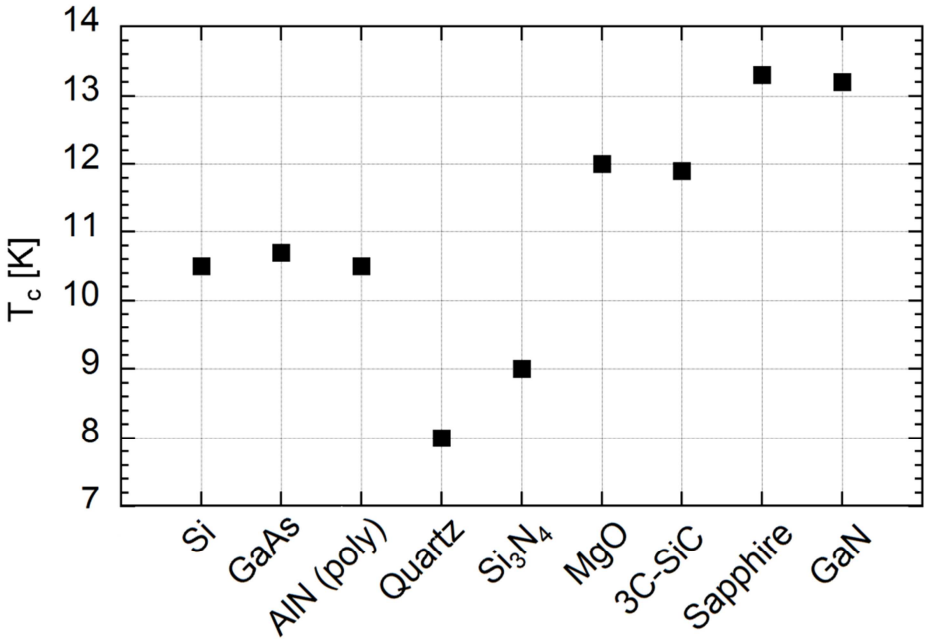

Figure 18: Highest reported critical temperature of NbN film with thicknesses between 3.5 and 6 nm, references see Table 2

MgO, 3C-SiC, sapphire and GaN have proven to yield single crystal NbN films with T_c between 11.9 K and 13.3 K. However, fabrication challenges may appear

with the use of MgO buffer-layer and substrates because of their hydrophobic character. Sapphire on the other hand causes problems due to its hardness and is therefore difficult to integrate in waveguide based applications at submillimeter and THz frequencies. 3C-SiC was first demonstrated in 2007 [52], although since then no report has made about a device utilizing the NbN/SiC material combination which may be due to unreliability in the deposition process. The high T_c that is achieved with the GaN buffer-layer is a very recent discovery [Paper A] and has yet to prove the prospective improvements on technologies based on ultra-thin NbN. Therefore, the next section will particularly focus on the advantages that come along with the use of this buffer-layer.

3.5 $Al_xGa_{1-x}N$ buffer-layers for NbN THz electronics

The growth of high quality AlGaN epilayers has been subject to intense research for many years now due to their use in optoelectronics and high-power RF devices. Metal-organic chemical vapor deposition (MOCVD) is usually used to grow such layers. Nitrogen gas is bubbled trough a liquid precursor such as Trimethylaluminium, respectively Trimethylgallium and is transported to the reaction chamber where it chemically reacts at the substrates surface and provides conditions for the crystal growth. Sapphire substrates are commonly employed due to their large wafer size, price and availability. Others such as SiC, Si, freestanding GaN or AlN can also be used as a substrate to grow high quality AlGaN layer which serve equally to provide the single crystal growth of NbN with T_c of approximately 13 K as illustrated in Figure 19.

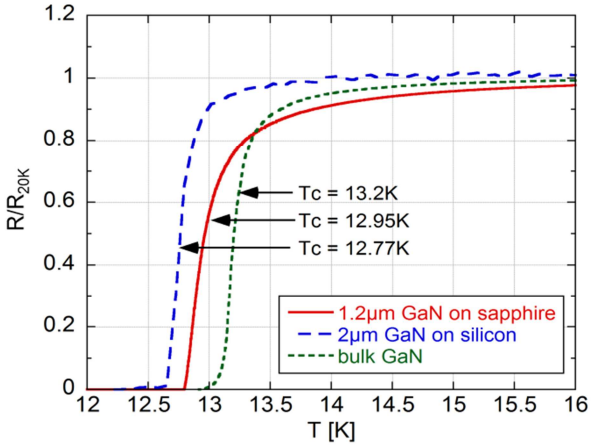

Figure 19: Normalized resistance versus temperature of a 5 nm thin NbN film deposited onto a GaN buffer—layer, which itself was grown onto sapphire, Si substrates as well as bulk GaN

The GaN buffer-layer to grow onto NbN is particularly useful for phonon cooled HEB mixers since it yields excellent superconducting properties as compared to e.g. Si substrates as illustrated in Figure 21a. The use of GaN buffer-layer allows

for a reduction of the NbN film thickness without suppressing the T_c significantly, and in consequence results in the decrease of the phonon escape time.
The phonon transmissivity may also be increased as suggested in Figure 11, resulting in an improved acoustic matching between film and substrate. Moreover, the interface possesses only very few defects as it is indicated by HRTEM and HAADF/STEM in Figure 20a,c and should therefore reduce the effect of phonon trapping at the film/substrate boundary as described in chapter 2.3.3.

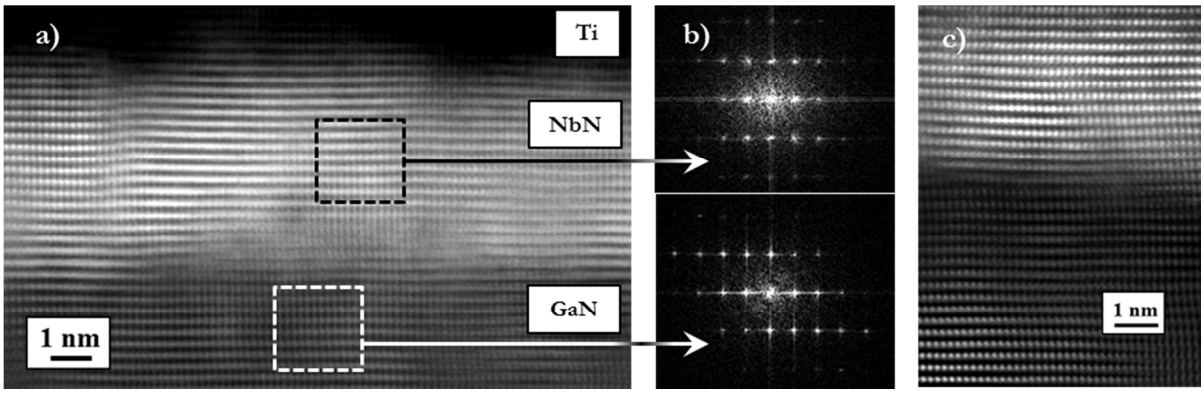

Figure 20: a) Epitaxial growth of NbN onto the GaN buffer-layer, the Ti top layer served as a contrast for better visibility. b) Diffraction pattern from FFT taken of the selected areas inside the NbN film and GaN layer. c) Very few stackfaults are visible at the interface [Paper A].

This strongly points towards an improvement of the IF bandwidth of the NbN HEB mixer due to the effective heat transfer across the film/substrate interface. From an electrical point of view, GaN features very low loss at submillimeter and THz frequencies [85] and its dielectric constant of 8.9 allows for a compact design.

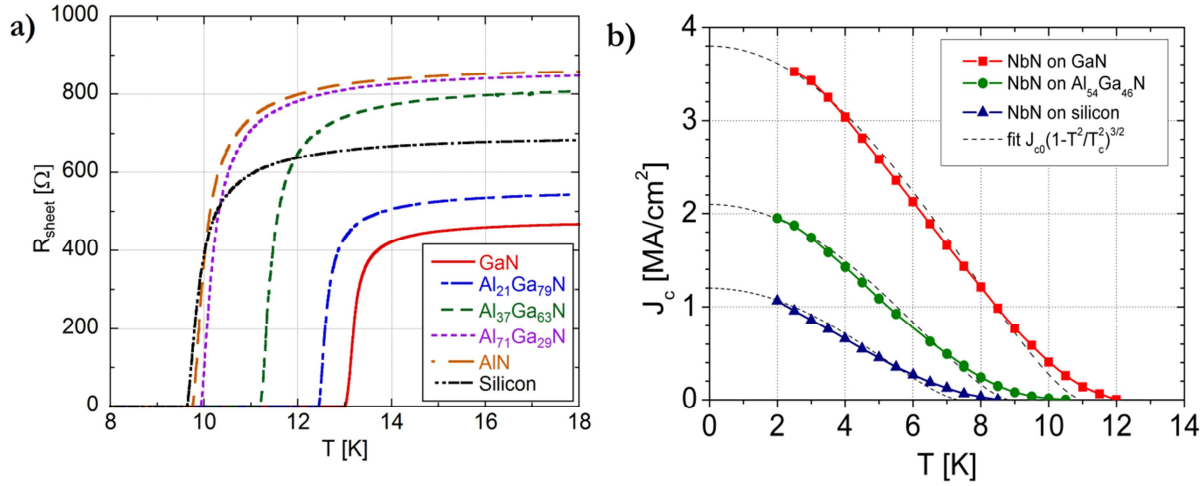

Figure 21: a) Resistance versus temperature behavior of ultra-thin NbN films with 5 nm thickness, deposited on the AlGaN buffer-layer in comparison with Si substrates b) Critical current density versus temperature for NbN grown onto GaN Al54Ga46N and Si substrates.

Furthermore, the high critical current density of NbN/GaN of 3.8 $MAcm^{-2}$ as compared to NbN grown on Si substrates with 1.2 $MAcm^{-2}$ [Paper A], see Figure 21b, justifies its use in other applications such as SIS junctions, SQUIDs or superconducting IF circuitry. In e.g. multi-layer fabrication processes it is often necessary to avoid high temperatures. Therefore, the ambient deposition of NbN onto GaN was considered and showed still improved properties over NbN/Si deposited at high substrate temperatures [Paper B].

4
HEB IF bandwidth study

4.1 Experiment description

The influence of the GaN buffer-layer on the escape time of a phonon cooled NbN HEB mixer operating at 180 GHz is investigated and compared to commonly used Si substrates. In this relatively low frequency band, sufficient RF power is available and the radiation can be coupled into the bolometer without the need of a quasi-optical arrangement (antenna and lens) or a waveguide mount (electrical probe and appropriate thin film structures), which eases the fabrication and allows for the characterization of different substrates in a timely manner.
The IF bandwidth of practical micro sized HEBs is not only determined by the NbN film characteristics, also electro-thermal feedback associated with self-heating in the HEB bridge plays a role and causes different IF bandwidths upon the change of its bias conditions [33]. The bias point that provides the lowest noise temperature of the HEB is therefore relevant when stating the IF bandwidth performance of such mixers.
In our experiment, however, the bath temperature is increased by warming up the whole mixer block close to the critical temperature of the NbN film. This has several important implications such as the temperature of the film lattice is close to the one of electrons and yields therefore a bolometric response. The electron-phonon interaction time is believed to be very short as it is proportional to $T^{-1.6}$ for NbN films [41] and thus, is negligible compared to the temperature-independent phonon escape time. This particular mode of operation allows therefore to investigate the effect of buffer-layers and film thickness in a simplified manner. Moreover, the bolometric response caused by the heating of the HEB, will also reduce the influence of electro-thermal feedback, the bias dependence on IF

bandwidth as well as the requirement of LO power. Finally, the operational frequency of around 180 GHz is rather low for NbN films with T_c above 13 K but by elevating the temperature we reach the situation when the quanta size is sufficient to effectively produce quasiparticles.
The experimental setup is depicted in Figure 22.

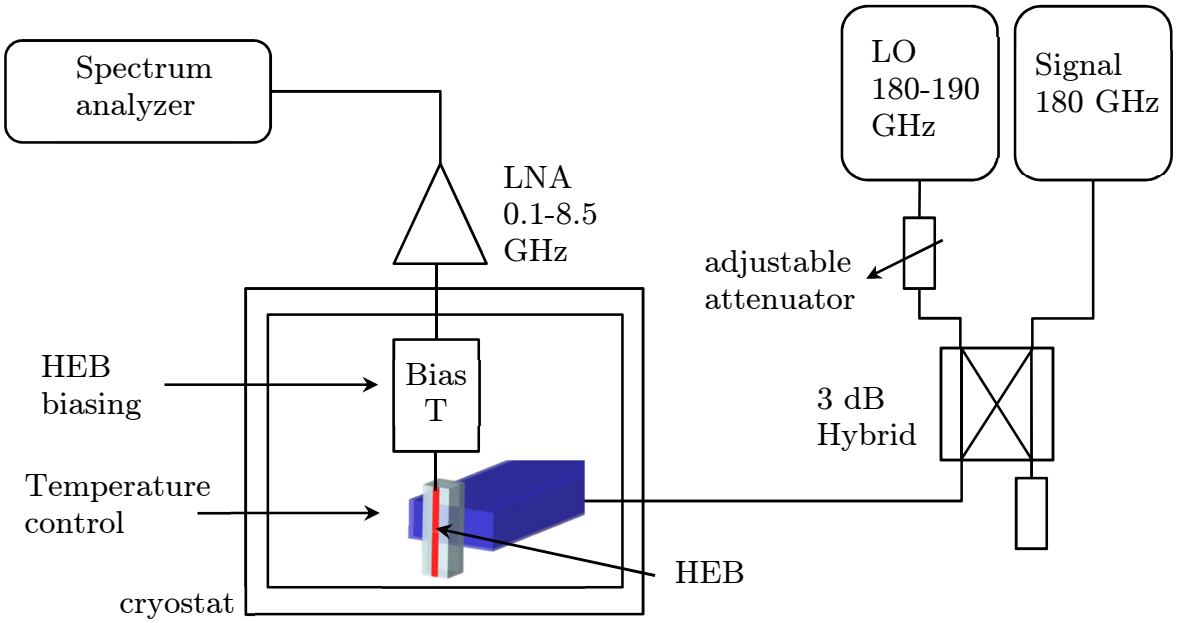

Figure 22: Measurement setup for IF roll-off investigation which is accompanied with the phonon escape from the NbN film to the buffer-layer/substrate when operated in the bolometric regime.

The RF and local oscillator signal are combined in a 3 dB hybrid and guided into the cryostat via waveguides. The generated IF signal is amplified by a wideband LNA and measured in a spectrum analyzer.

4.2 Characterization of the measurement system

In order to conclusively evaluate the influence of the used buffer-layer on the HEB IF bandwidth, it is important to exclude external effects that alter the IF response. Such measurement uncertainties can be caused by e.g. losses in the cables or standing waves attributed to the impedance mismatch. This is a severe problem especially for measurements performed at cryogenic temperatures since the impedance of e.g. coaxial cables is normally specified at room temperature and is likely to change due to the thermal contractions of the dielectric material at colder temperatures. Thus, careful calibration of all involved IF circuits, as seen in Figure 23 is essential.

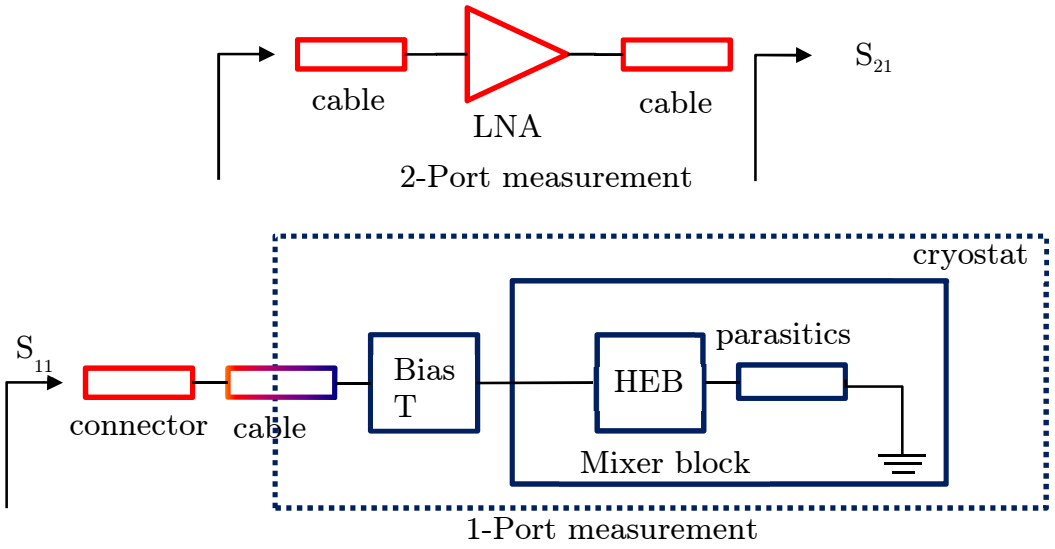

Figure 23: Components of the IF chain to be calibrated.

The frequency behavior of all components of the IF chain were assessed with a calibrated vector network analyzer (VNA), utilizing the time domain reflectometry and gating technique. Since the impedance of the HEB mixer can be varied in a wide range by changing its operating point, it could be used as a calibration standard such as a short (superconducting state), a load (normal state) or an open termination (e.g. destroyed device). S-parameter measurements at these operating points supported by an electrical circuit simulation enabled the characterization of the entire IF chain in the frequency range of interest as presented in the Figure 24.

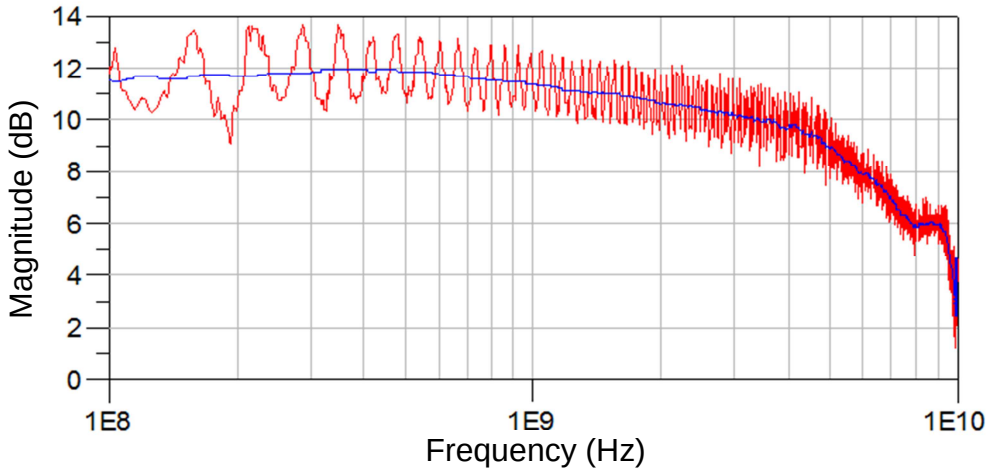

Figure 24: Transfer function of the entire IF system, including the LNA and the HEB impedance in its operating point.

The aforementioned standing waves are predicted to have an amplitude of approximately 3 dB, its ripple frequency is proportional to the electrical length between the DUT (HEB) and the spectrum analyzer.

It can be seen that the measurement system has a relatively sharp system roll-off at 4 GHz which is mainly caused by the increasing losses in the coaxial cables with rising IF frequency.

4.3 Measurement results

Measurements of two different NbN films with different superconducting and structural properties as stated in Table 3 were conducted.

Table 3: Summary of the properties of the investigated samples used for the HEB fabrication

substrate	thickness	T_c	R_{sq} at 20 K	Bolometer	
	[nm]	[K]	[Ohm]	R_{DC} at 20 K [Ω]	Size [μm^2]
Silicon	5	9	620	65	5*60
GaN on sapphire	5	12	550	60	5*40

The IF level was recorded from 100 MHz up to 8 GHz as illustrated in Figure 26. As expected the recorded data shows evidence of standing waves, with amplitude about 3 dB. It was not possible to reconstruct the period of the standing wave due to the limited amount of measurement points. However, based on the known frequency behavior of the IF chain it was possible to correct the recorded raw data according to Figure 26.

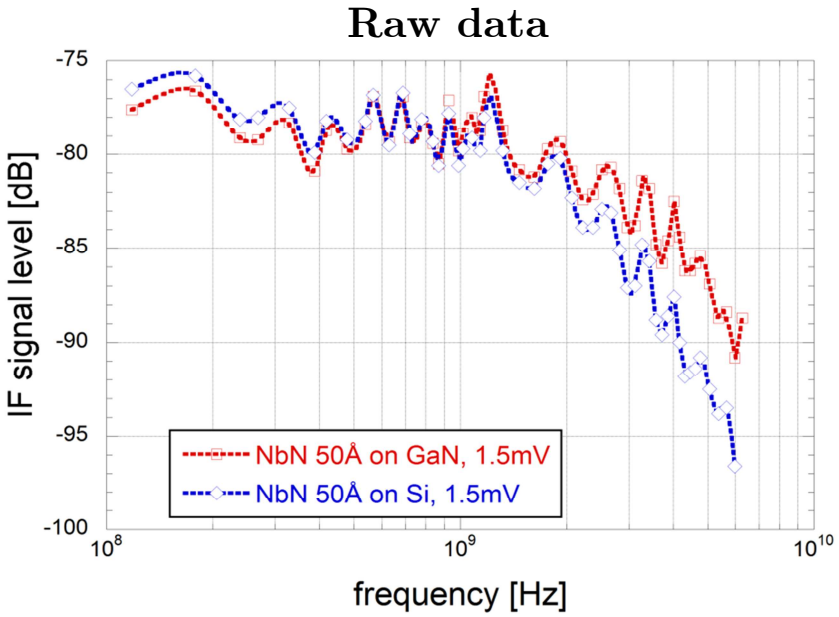

Figure 25: Measured IF signal level without correction for IF chain response.

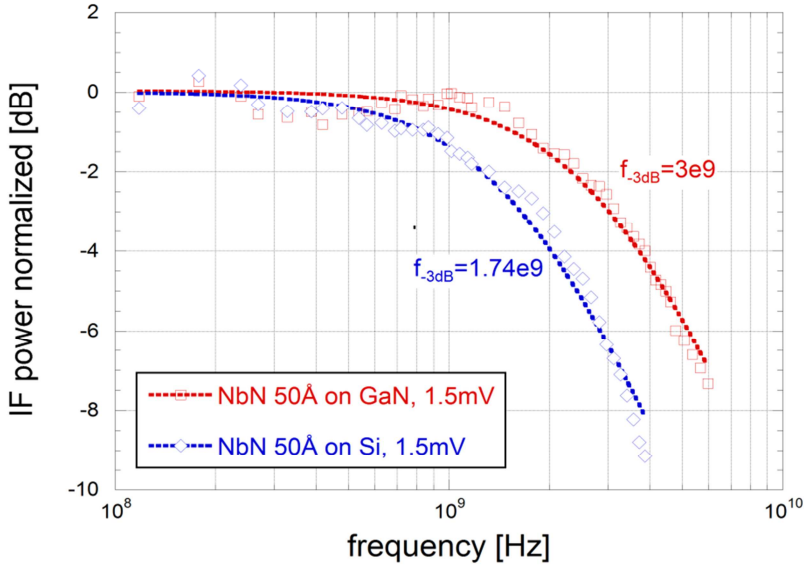

Figure 26: Measured IF signal level (normalized) with correction for IF chain response.

The corrected data shows a clear increase in IF roll-off frequency from 1.74 GHz for the Si substrate to 3 GHz on the GaN buffer-layer for NbN films with identical thickness of 5 nm. The dashed lines in Figure 26 represent the theoretical fit according to (17) and coincide very well with the measurement data which supports the reliability of this measurement system for the time efficient characterization of IF bandwidth of HEBs.

$$A_{IF}(f)_{dB} = A_{0,dB} \cdot \left(1 - \left(\frac{f}{f_{3dB}}\right)^2\right) \tag{17}$$

Furthermore, the influence of the IF response on different bias conditions and bath temperatures have been investigated and are presented in Figure 27.

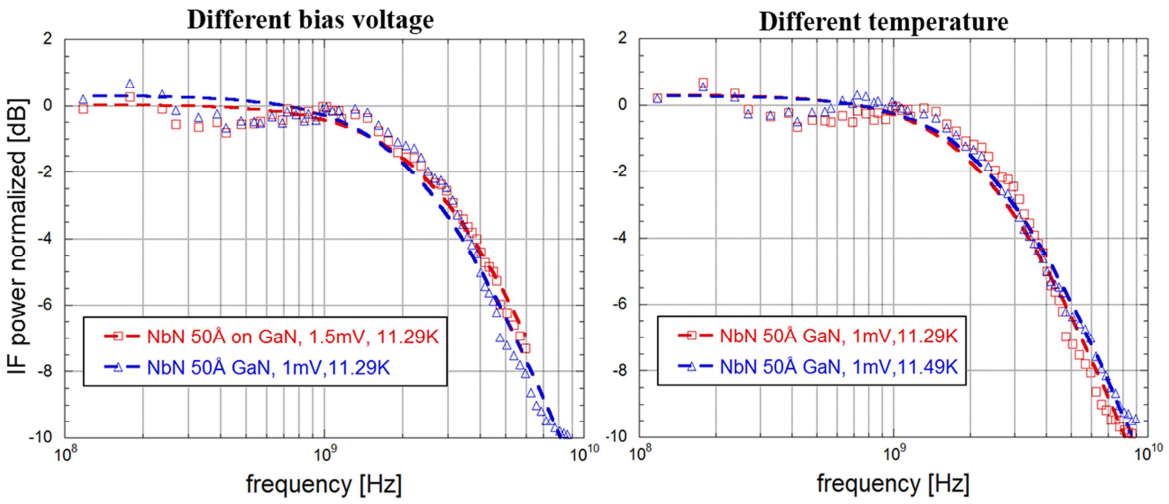

Figure 27: Normalized and corrected IF signal level for 5nm NbN/GaN at different bias voltage and temperature

The frequency response is almost identical and supports the assumption of negligible electro-thermal feedback and the presence of a bolometric response with similar temperatures of electrons and film lattice.
The extracted IF roll-off cannot directly be compared to the IF bandwidth obtained with practical HEB mixers because of the raised temperature of the bath, the large bolometer area as well as the reduced electro-thermal feedback. Nonetheless, the comparative measurement points strongly towards the prospective improvement of IF bandwidth with the employment of NbN ultra-thin film grown onto GaN buffer-layers that is expected to take place due to an enhancement of the phonon escape.

5
Concluding remarks

This thesis dealt with the development of ultra-thin NbN films with improved superconducting properties, particularly suited for HEB applications with at enhanced IF bandwidth.
As a result, the hexagonal buffer-layer $Al_xGa_{1-x}N$ was employed for the first time and yield NbN films deposited by reactive DC magnetron sputtering with 13.2 K critical temperature on the GaN epi-layer despite its thickness of only 5 nm. Excellent homogeneity, a very distinct interface and the epitaxial growth were confirmed by HRTEM investigation. The critical current was determined to be 3.8 MA/cm^2 and therefore three fold compared to a high quality NbN film deposited onto a Si substrate. The GaN buffer-layer can therefore also be employed in other superconducting electronics such as SIS tunnel junctions or SSPDs which would benefit from high quality NbN films in order to extend the operational bandwidth or sensitivity, respectively.
With changing the Al content x in the $Al_xGa_{1-x}N$ compound, it was possible to modify the superconducting properties of the NbN such as the T_c which slowly deteriorated with increasing the Al content above 20% down to 10.5 K, exhibiting a poly-crystalline crystal structure.
The characterization with XPS and REELS techniques revealed the presence of the semiconductor like NbO_2 at the surface of NbN when exposed to ambient air, which is in contrast to the previously believed insulating Nb_2O_5 that forms on Nb surfaces or thick NbN films under thermal oxidation.
Furthermore, it was suggested that the NbN/GaN material combination provides a better acoustic match compared to commonly used substrates such as Si or MgO and thus enhancing the IF bandwidth of phonon cooled HEBs. Preliminary results that were obtained from a mixer experiment at 180 GHz point strongly towards this trend as the IF signal roll-off was increased by almost 80 % in presence of the GaN buffer-layer compared to bare silicon.

The continuous improvement of HEB mixers for THz applications is essential since there is no other competing technology with similar noise performance up to now. Thus, the next step is to proof the expected performance increase of IF bandwidth that comes with the employment of the GaN buffer-layer in a practical HEB mixers working at THz frequencies.

6
Summary of appended papers

Paper A

Epitaxial growth of ulta-thin NbN films on AlxGa1-xN buffer-layers

In this paper, the possibility to grow single crystal ultra-thin NbN films onto $Al_xGa_{1-x}N$ buffer-layers is shown for the first time. Electrical and structural properties of the resulting NbN film are presented and compared to commonly used substrates.

Paper B

Ambient temperature growth of mono- and polycrystalline NbN nanofilms and their surface and composition

The growth of single crystal NbN films by reactive DC magnetron sputtering in the absence of a substrate heating on GaN buffer-layers was demonstrated. The native oxide of NbN ultra-thin films was identified with XPS and REELS techniques to be NbO_2, which has direct implications on the surface treatment.

Bibliography

[1] E. Gershenzon, G. Gol'tsman, I. Gogidze, A. Elant'ev, B. Karasik and A. Semenov, "Millimeter and submillimeter range mixer based on electronic heating of supercondcuting films in the resistive state," *Sov. Phys. Superconductivity,* vol. 3, p. 1582, 1990.

[2] A. v. Helden, S. Dupré, R. van Gent and H. Zuidervaart, The origins of the telescope, Amsterdam: KNAW Press, 2010.

[3] "Atacama Pathfinder EXperiment APEX," ESO, Max-Planck-Institut für Radiastronomie, Onsala Rymdobservatorium, 08 2015. [Online]. Available: http://www.apex-telescope.org/. [Accessed 01 2016].

[4] "Arizona Radio Observatory - SMT," Arizona Radio Observatory, 29 08 2014. [Online]. Available: http://aro.as.arizona.edu/. [Accessed 01 2016].

[5] D. Marrone, R. Blundell, E. Tong, S. Paine, D. Loudkov, J. Kawamura, D. Luhr and C. Barrientos, "Observations in the 1.3 and 1.5 THz atmospheric windows with the Receiver Lab Telescope," in *16th International Symposium on Space Terahertz Technology*, Gothenburg, 2005.

[6] "Atacama Large Millimeter/submillimeter Array," ESO, NAOJ, NRAO, [Online]. Available: http://www.almaobservatory.org/en/home. [Accessed 01 2016].

[7] D. Leisawitz, "Scientific motivationand technology requirements for the SPIRIT and SPECS far-infrared/submillimeter space interferometers," *Proc. SPIE,* vol. 4013, pp. 36-46, 2000.

[8] S. Withington, "THz technology for astronomy," in *IEE Colloquium on Terahertz technology*, London, 1995.

[9] C. o. A. o. S. f. Transportation, Assessment of Millimeter-Wave and Terahertz Technology for Detection and Identification of Concealed Explosives and Weapons, Washington, DC: The National Academies Press, 2007.

[10] J. Tucker, "Quantum limited detection in tunnel junctions," *J. Quantum Electron.,* Vols. QE-15, pp. 1234-1258, 1979.

[11] E. Geshenzon, M. Gershenzon, G. Gol'tsman, A. Semenov and A. Sergeev, "Heating of quasiparticles in a superconducting film in the resistive state," *JETP Lett.,* vol. 34, no. 5, pp. 268-271, 1981.

[12] P. Y. Aghdam, "Characterisation of the Specific Capacitance of

Superconducting Tunnel Juntions," Chalmers Univeristy of Technology, Gothenburg, 2015.

[13] I. Konstantin, A. Stockhausen, M. Siegel, A. Semenov, H. Richter and H. Hübers, "NbN HEB for THz Radiation: Technological Issues," in *19th International Symposium on Space Terahertz Technology*, Groningen, 2008.

[14] T. May, G. Zieger, S. Anders, V. Zakosarenko, M. Starkloff, H. Meyer, G. Thorwirth and E. Kreysa, "Passive stand-off terahertz imaging with 1 hertz frame rate," in *Terahertz for Military and Security Applications*, Orlando, 2008.

[15] K. Ishigaki, M. Shiraishi, S. Suzuki and M. Asada, "Direct intensity modulation and wireless data transmission characteristics of terahertz-oscillating resonant tunnelling diodes," *Electronics Letters,* vol. 48, no. 10, pp. 582-583, 2012.

[16] G. Aschermann, E. Friederich, E. Justi and J. Kramer, Supraleitfähige Verbindungen mit extrem hohen Sprungtemperaturen (NbH und NbN), Berlin: Springer Berlin Heidelberg, 1943.

[17] J. R. Gavaler, J. K. Hulm, M. A. Jankocko and C. K. Jones, *J. Vac. Sci. Technol.,* vol. 6, p. 177, 1969.

[18] G. Oya and Y. Onodera, *J. Appl. Phys.,* vol. 45, p. 1389, 1974.

[19] R. Roy, P. F. Carcia, R. Messier and D. Rogowski, *Mater. Res. Bull.,* vol. 10, p. 379, 1975.

[20] M. W. William, K. M. Ralls and M. R. Pickus, *J. Phys. Chem. Solids,* vol. 28, p. 333, 1967.

[21] B. Scheerer, Preparation of NbN Single Crystals, Karlsruhe: Kernforschungszentrum Karlsruhe, 1979.

[22] G. Brauer and R. Esselborn, "Nitridphasen des Niobs," *Journal of Inorganic and General Chemistry,* vol. 309, no. 3-4, pp. 151-170, 1961.

[23] A. Khudchenko, A. Baryshev, K. Rudakov, V. Koshelets, P. Dmitriev, R. Hesper and L. Jong, "High Gap Nb-AlN-NbN SIS junctions for frequency Band 790-950 GHz," in *26th International Symposium on Space Terahertz Technology*, Cambridge, MA, 2015.

[24] M. Takeda, Y. Uzawa and Z. Wang, "SIS Mixers Based on NbN Techniques for ALMA Band 10," *Applied Superconductivity,* vol. 17, no. 2, pp. 359-362, 2007.

[25] Y. Korneeva, I. Florya, A. Semenov, A. Korneev and G. Gol'tsman, "New Generation of Nanowire NbN Superconducting," *IEEE Transactions on Applied Superconductivity,* vol. 21, no. 3, pp. 323-326, 2011.

[26] M. Aurino, E. Baggetta, S. Bouat, V. Michal, D. Renaud, C. Bornier, M. Laine and J. Villegier, "Cryogenic Test-Bed Applied to 9 K NbN RSFQ," *Applied Superconductivity,* vol. 21, no. 3, pp. 904-907, 2011.

[27] N. Balkan and S. Luryi, "Hot Electrons in smeiconductor devices," in *Hot Electrons in Semiconductors*, Oxford, Clarendon Press, 1998, pp. 386-387.

[28] K. Il'in, I. Milostnaya, A. Verevkin, G. Gol'tsman, E. Gershenzon and R. Sobolewski, "Picosecond hot-electron energy relaxation in NbN superconducting photodetectors," *Applied Physics Letter,* vol. 76, no. 19, 2000.

[29] D. W. Floet, J. R. Gao, T. M. Klapwijk and P. A. J. Korte de, "Bias Dependence of the Thermal Time Constant in Nb," in *International Symposium on Space and Terahertz Technology*, 2000.

[30] I. K., M. Lindgren, M. Currie, A. Semenov, G. Gol'tsman and R. Sobolewski, "Picosecond hot-electron energy relaxation in NbN superconducting photodetectors," *Applied Physics Leters,* vol. 76, no. 19, 2000.

[31] S. Bevilacqua, E. Novoselov, S. Cherednichenko, H. Shibata and Y. Tokura, "MgB2 Hot-Electron Bolometer Mixers at Terahertz Frequencies," *Applied Superconductivity,* vol. 25, no. 3, 2015.

[32] N. Perrin and C. Vanneste, "Dynamic behaviour of a superconductor under time-dependent external excitation," *J. Phys. France,* vol. 48, no. 8, pp. 1311-1316, 1987.

[33] J. Kooi, J. Baselmans, M. Hajenius, J. Gao, T. Klapwijk, P. Dieleman, A. Baryshev and G. de Lange, "IF Impedance and Mixer Gain of NbN Hot-Electron Bolometers," *Journal of Applied Physics,* vol. 101, p. 044511, 2007.

[34] A. Sergeev, B. S. Karasik, M. Gershenson and V. Mitin, "Electron-phonon scattering in disordered metallic films," *Physica B,* no. 316-317, pp. 328-330, 2002.

[35] H. Bottger, Principles of the Theory of Lattice Dynamics, Berlin: Physica-Verlag, 1983.

[36] M. Y. Reizer and A. V. Sergeev, "Electron-Phonon interaction in impure metals and superconductors," *Sov. Phys. JETP,* vol. 63, no. 3, pp. 1056-1070, 1986.

[37] A. Schmid, "Electron-Phonon Interaction in an Impure Metal," *Z. Physik,* vol. 259, no. 5, pp. 421-436, 1973.

[38] Y. F. Komnik, V. Y. Kashirin, B. I. Belevtsev and E. Y. Beliaev, "Temperature variation of the time of inelastic electron relaxation in disordered bismuth films," *Physical Review B,* vol. 50, no. 20, 1994.

[39] S. P. Chockalingam, M. Chand, J. Jesudasan, V. Tripathi and P. Raychaudhuri, "Superconducting properties and Hall effect of epitaxial NbN thin films," *Physical Review B,* vol. 77, 2008.

[40] N. G. Ptitsina, G. M. Chulkova, K. S. Il'in, A. V. Sergeev, F. S. Pochinkov and E. M. Gershenzon, "Electron-phonon interaction on disordered metal films: The resistivity and electron dephasing rate," *Physical Review B,* vol. 56, no. 16, pp. 10089-10096, 1997.

[41] Y. Gousev, G. Gol'tsman, A. Semenov, E. Gershenzon, R. Nebosis, M. Heusinger and K. Renk, "Broadband ultrafast superconducting NbN detector for electromagnetic radiation," *Journal of Applied Physics,* vol. 75, no. 7, pp. 3695-3697, 1994.

[42] S. P. Chockalingam, "Superconducting properties and Hall Effect of epitaxial NbN thin films".

[43] A. Ghosh, H. Weisman, M. Gurvitch, H. Lutz, O. Kammerer, C. Snead, A. Goland and M. Strongin, "The effects of irradiationat cryogenic temperatures and electron irradtion on Tc and the transport properties of A-15 supercondcutors.," *Journal of Nuclear Materials,* vol. 72, pp. 70-75, 1979.

[44] L. Kang, B. Jin, X. Liu, X. Jia and J. Chen, "Suppression of superconductivity in epitaxial NbN ultrathin films," *Journal of Applied Physics,* vol. 109, 2011.

[45] R. Da-Hua and C. Xin-Lu, "First-principles calculations on the elastic and thermodynamic properties of NbN," *Chin. Phys. B,* vol. 21, no. 12, 2012.

[46] T. Amrioua, Bouhafsa, B., H. Aouraga, B. Khelifab, S. Bresson and C. Mathieu, "FP-LAPW investigations of electronic structure and bonding mechanism of NbC and NbN compounds," *Physica B,* vol. 325, pp. 46-56, 2003.

[47] J. Kim, J. Achenbach, P. Mirkarimi, M. Shinn and S. Barnett, "Elastic constants of single-crystal transition-metal nitride films measured by line-focus acoustic microscopy," *Journal of Applied Physics,* vol. 72, p. 1805, 1992.

[48] Z.-H. Wang, X.-Y. Kuang, X.-F. Huang, P. Lu and A.-J. Mao, "Pressure-induced structural transition and thermodynamic properties of NbN and effect of emtallic bonding on its hardness," *EPL,* vol. 92, 2010.

[49] W. A. Little, "The transport of heat between dissimilar solids at low temperatures," *Can. J. Phys.,* vol. 37, no. 334, 1959.

[50] S. B. Kaplan, "Acoustic Matching of Superconducting Films to Substrates," *Journal of Low Temperature Physics,* vol. 37, pp. 343-364, 1979.

[51] D. Dochev, V. Desmaris, A. Pavolotsky, D. Meledin, Z. Lai, A. Henry, E. Janzen, E. Pippel, J. Woltersdorf and V. Belitsky, "Growth and characterization of epitaxial ultra-thin NbN films on 3C-SiC/Si substrates for terahertz applications," *Supercond. Sci. Technol.,* 2011.

[52] J. Gao, M. Hajenius, F. Tichelaar, T. Klapwijk, B. Voronov, E. Grishin, G. Goljtsman, C. Zorman and M. Mehregany, "Monocrystalline NbN nanofilms on a 3C-SiC/Si substrate," *Applied Physics Letters,* vol. 91, p. 062504, 2007.

[53] R. E. d. Lamaestre, P. Odier, E. Bellet-Amalric, P. Cavalier, S. Pouget and J.-C. Villegier, "High quality ultrathin NbN layers on sapphire for superconducting single photon detectors," *Journal of Physics: Conference Series,* vol. 97, p. 012046, 2008.

[54] M. Kaganov, I. Lifshitz and L. Tanatarov, "Relaxation between electrons and the crystalline lattice," *Soviet physics. JETP,* vol. 4, no. 2, p. 173, 1957.

[55] J. Ziman, Electrons and Phonons, Oxford: Oxford University Press, 1960.

[56] X. Li and R. Yang, "Effect of lattice mismatch on phonon transmission and interface thermal conductance across dissimilar material interfaces," *Physical Review B,* vol. 86, 2012.

[57] S. Bedorf, Development of Ultrathin niobium Nitride and Niobium Titanium

Nitride Films for THz Hot-Electron Bolometers, Cologne: Universität Köln, 2005.

[58] A. Linde, R. Marin-Ayral, D. Granier, F. Bosc-Rouessac and V. Grachev, "Synthesis of cubic niobium nitride by reactive diffusion under nitrogen pressure," *Materials Research Bulletin,* vol. 44, no. 5, pp. 1025-1030, 2009.

[59] F. Mercier, S. Coindeau, S. Lay, A. Crisci, M. Benz, T. Encinas, R. Boichot, A. Mantoux, C. Jimenez, F. Weiss and E. Blanquet, "Niobium nitride thin films deposited by high temperature chemical vapor deposition," *Surface and Coatings Technology,* vol. 260, pp. 126-132, 2014.

[60] G. Zou, M. Jain, H. Zhou, H. Luo, S. Baily, L. Civale, E. Bauer, T. McCleskey, A. Burrell and Q. Jia, "Ultrathin epitaxial superconducting niobium nitride films grownby a chemical solution technique," *Chemical Communications,* pp. 6022-6024, 2009.

[61] K. Nakamura, M. Hikita, H. Asano and A. Terada, "Reactive Synthesis of Niobium Nitride by Pulse Laser Annealing," *Japanese Journal of Applied Physics,* vol. 21, no. 1, pp. 672-673, 1982.

[62] R. Treece, J. Horwith, J. Claassen and D. Chrisey, "Pulsed laser deposition technique of high-quality NbN thin films," *Applied Physics Letters,* vol. 65, no. 22, pp. 2860-2862, 1994.

[63] K. Kawaguchi and M. Sohma, "Preparation of Superconducting Niobium Nitride Films by Molecular Beam Epitaxy Method," *Japanese Journal of Applied Physics,* vol. 30, no. 12, pp. 2088-2090, 1991.

[64] P. Alén, M. Ritala, K. Arstila, J. Keinonen and M. Leskelä, "The Growth and Diffusion Barrier Properties of Atomic Layer Deposited NbNx Tin Films," *Thin Solid Films,* vol. 491, no. 1-2, pp. 235-241, 2005.

[65] D. W. Capone, K. E. Gray and R. T. Kampwirth, "New scaling relation for sputtered NbN films," *J. Appl. Phys.,* vol. 65, no. 1, pp. 258-261, 1989.

[66] F. J. Cadieu and N. Chencinski, "Selective thermalization in sputtering to produce high Tc films," *IEEE Transactions on Magnetics,* vol. 11, no. 2, pp. 227-230, 1975.

[67] Z. Wang, A. Kawakami, Y. Uzawa and B. Komiyama, "Superconducting properties and crystal structures of singlecrystal niobium," *J. Appl. Phys.,* vol. 79, no. 10, pp. 7837-7842, 1996.

[68] M. Kroug, S. Cherednichenko, M. Choumas, H. Merkel, E. Kollberg, H. Hübers, H. Richter, D. Loudkov, B. Voronov and G. Gol'tsman, "HEB Quasi-optical Heterodyne Receiver for THz Frequencies," in *12th Inernational Symposium on Space and Terahertz Technology*, 2001.

[69] S. Miki, Y. Uzawa, A. Kawakami and Z. Wang, "IF bandwidth and Noise Temperature Measurements of NbN HEB Mixers on MgO Substrates," *Applied Superconductivity,* vol. 11, no. 1, p. 175, 2001.

[70] H. Merkel, P. Khosropanah, K. Yngvesson, S. Cherednichenko, M. Kroug, A. Adam and E. Kollberg, "An active zone small signal model for hot electron bolometric mixers," in *12th International Symposium on Space and Terahertz*

Technology, 2001.

[71] J. Baselmans, M. Hejenius, J. Gao, T. Klapwijk, P. de Korte, B. Voronov and G. Gol'tsman, "Noise performance of NbN Hot Electron Bolometer mixers at 2.5 THz," in *14th International Symposium on Space and Terahertz Technology*, 2003.

[72] T. Aggarwal, P. Khosropanah, W. Zhang, F. Tichelaar, J. Gao and T. Klapwijk, "Superconducting contacts and NbN HEB mixer," in *19th International Symposium on Space and Terahertz Technology*, Groningen, 2008.

[73] A. Ermolieff, M. Girard and C. Raoul, "An XPS comparative study on thermal oxide barrier formation on Nb and NbN thin films," *Applications of Surface Science,* vol. 21, p. 65, 1985.

[74] R. Frankenthal, D. Siconolfi, W. Sinclair and D. Bacon, "Thermal Oxidation of Niobium Nitride Films at Temperatures from 20-400 flC," *J. Electrochem. Soc.: Solid-State Science and Technology,* vol. 130, no. 10, 1983.

[75] P. Gallagher, W. Sinclair, D. Bacon and G. Kammlott, "Oxidation of sputtered niobium nitride films," *J. Electrochem. Soc.: Solid-State Science and Technology,* vol. 130, no. 10, 1983.

[76] D. Bach, EELS investigations of stoichiometric niobium oxides and niobium-based capacitors, Karlsruhe: Universität Karlsruhe, 2009.

[77] W. Slysz, M. Guziewicz, M. Borysiewicz, J. Domagala, I. Pasternak, K. Hejduk, W. Rzodkiewicz, J. Ratajczak, J. Bar, M. Wegrzecki, P. Grabiec, R. Grodecki, I. Wegrzecka and R. Sobolewski, "Ultrathin NbN Films for Superconducting," in *VIII International Conference ION*, Kazimierz Dolny, 2010.

[78] B. Karasik, G. Gol'tsman, B. Voronov, S. Svechnikov and E. Gershenzon, "Hot Electron Quasioptical NbN . Superconducting Mixer," *Applied Superconductivity,* vol. 5, no. 2, pp. 2232-2235, 1995.

[79] M. Frommberger, P. Sabon, M. Schicke and K. Schuster, "Characterization of NbN Thin Films produced on Quartz Substrates using MgO Seed Layers for phonon cooled Hot-Electron Bolometer Devices," in *12th International Symposium on Space Terahertz Technology*, 2001.

[80] D. Meledin, E. Tong, R. Blundell, N. Kaurova, K. Smirnov, B. Voronov and G. Gol'tsman, "Study of the IF Bandwidth of NbN HEB Mixers," *Applied Superconductivity,* vol. 13, no. 2, pp. 164-167, 2003.

[81] F. Marsili, A. Gaggero, L. Li, A. Surrente, R. Leoni, F. Levy and A. Fiore, "High quality superconducting NbN thin," *Superconductor Science and Technology,* vol. 22, no. 9, 2009.

[82] X. Q. Jia, L. Kang, M. Gu, X. Z. Yang, C. Chen, X. C. Tu, B. B. Jin, W. W. Xu, J. Chen and P. H. Wu, "Fabrication of a strain-induced high performance NbN ultra-thin film by a Nb5N6 buffer layer on Si substrate," *Supercond. Sc. Technol.,* vol. 27, p. 035010, 2014.

[83] J. Zhang, X. Su, L. Zhang, L. Zheng, X. Wang and L. You, "Improvement of

the superconducting properties of NbN thin film on single-crystal silicon substrate by using a TiN buffer layer," *Supercond. Sci. Technol.,* vol. 26, no. 4, 2013.

[84] T. Shiino, S. Shiba, N. Sakai, T. Yamakura, L. Jiang, Y. Uzawa, H. Maezawa and S. Yamamoto, "Improvement of the critical temperature of superconducting NbTiN and NbN thin films using the AlN buffer layer," *Supercond. Sci. Technol.,* vol. 23, no. 4, 2010.

[85] W. Zhang, Azad, A. and D. Grischkowsky, "Terahertz studies of carrier dynamics and dielectric response of n-type, freestanding epitaxial GaN," *Appl. Phys. Lett.,* vol. 82, no. 17, pp. 2841-2843, 2003.